Quantifying functional phenotypes in human pluripotent stem cell derived cardiomyocytes for disease modelling and drug discovery

Meer, B.J. van

Abstract

Animal models are 78% accurate in determining whether drugs will alter contractility of the human heart. To evaluate the suitability of human-induced pluripotent stem cell-derived cardiomyocytes (hiPSC-CMs) for predictive safety pharmacology, we quantified changes in contractility, voltage, and/or Ca^{2+} handling in 2D monolayers or 3D engineered heart tissues (EHTs). Protocols were unified via a drug training set, allowing subsequent blinded multicenter evaluation of drugs with known positive, negative, or neutral inotropic effects. Accuracy ranged from 44% to 85% across the platform-cell configurations, indicating the need to refine test conditions. This was achieved by adopting approaches to reduce signal-to-noise ratio, reduce spontaneous beat rate to ≤ 1 Hz or enable chronic testing, improving accuracy to 85% for monolayers and 93% for EHTs. Contraction amplitude was a good predictor of negative inotropes across all the platform-cell configurations and of positive inotropes in the 3D EHTs. Although contraction- and relaxation-time provided confirmatory readouts forpositive inotropes in 3D EHTs, these parameters typically served as the primary source of predictivity in 2D. The reliance of these "secondary" parameters to inotropy in the 2D systems was not automatically intuitive and may be a quirk of hiPSC-CMs, hence require adaptations in interpreting the data from this model system. Of the platform-cell configurations, responses in EHTs aligned most closely to the free therapeutic plasma concentration. This study adds to the notion that hiPSC-CMs could add value to drug safety evaluation.

Chapter 6

Blinded, multi-centre evaluation of drug-induced changes in contractility using human induced pluripotent stem cell-derived cardiomyocytes

Modified after Toxicological Sciences 176, 103-123 (2020)

Berend van Meer#, Umber Saleem#, Puspita Katili, Nurul Mohd Yusof, Ingra Mannhardt, Ana Krotenberg, Leon Tertoolen, Tessa de Korte, Maria Vlaming, Karen McGlynn, Jessica Nebel, Anthony Bahinski, Kate Harris, Eric Rossman, Xiaoping Xu, Francis Burton, Godfrey Smith, Peter Clements, Christine Mummery, Thomas Eschenhagen, Arne Hansen, Chris Denning

# these authors contributed equally to this work

Introduction

On average, 37 new drugs are launched to market each year but cost of development has increased from approximately $14M per drug in the 1960s to approximately $1.5Bn now, inflation adjusted[1,2]. Attrition rates remain high, with only approximately 2% of the drugs entering phase 1 clinical trials actually progressing to use in patients. A key concern is cardiovascular toxicity, where acute, chronic, and comorbidity effects account for 17% of the 462 drugs withdrawn from market[3] and for 41% of the top 200 prescribed drugs being labeled with adverse drug reaction or black box warnings[4].

Altered cardiac electrophysiology was implicated in the withdrawal of 13 drugs from market between 1990 and 2006[5]. Such events led to International Conference on Harmonization (ICH) S7B guidelines for proarrhythmic risk detection using simplified *in vitro* assays to measure blockade of the rapid repolarization IKr current, commonly known as hERG[6]. Combined with ICH E14[7]guidelines on electrocardiogram monitoring, drug withdrawal due to electrical dysfunction has reduced, with no reported incidences since 2007. These approaches have improved safety, but the relatively poor specificity for predicting human outcomes and overconservativism of the assays has raised concern that promising drug candidates may be abandoned too early due to false positives[8].

Greater predictivity during the early stages of the drug development pipeline will require certain attributes from the chosen assays. These include being of human origin, suitable longevity for acute and chronic studies, compatible with medium-throughput analysis, reflective of working cardiomyocyte physiology and function, and compliant with 3Rs polices. This reduces the attractiveness or relevance of many existing systems, such as those involving animal models. This is also true for human- and animal-derived primary cardiomyocytes, which rapidly dedifferentiate in culture, lose viability, or become overrun with fibroblasts.

Alternative technologies are now showing potential in cardiovascular safety evaluation, with human-induced pluripotent stem cell-derived cardiomyocytes (hiPSC-CMs) as a key modality[9]. This is evidenced by their use in disease modeling, drug discovery and cardiac safety studies, which culminated in the Comprehensive *in vitro* Proarrhythmia Assay (CiPA) and Japanese iPS cardiac safety assessment initiatives[10-12]. Using CiPA as an example, the approach proposed was to identify proarrhythmic risk based on several key modalities including: (1) assessment of several major ion channels in transfected cell lines; (2) *in silico* modeling of the ion channel effects; (3) proarrhythmic assessment in hiPSC-CMs; and (4) clinical assessment of electrocardiograms from phase I human studies. Data that emerged from CiPA show that optical- and multielectrode array-based platforms using commercially sourced hiPSC-CMs enable an 87% accuracy in predicting proarrhythmic liability across geographically diverse testing laboratories[13], with similar studies being reported by others[14].

In contrast, there have been relatively few studies that have used hiPSC-CM contractility in predictive safety assessment[15]. This is surprising because cardiovascular liability of drugs occurs commonly via altered function of the contractile myocardium. Also, monitoring contractility in hiPSC-CMs is currently being done at low throughput or by

using surrogate markers (eg, impedance) and, so far, there has been no detailed cross-site validation study to accurately assess the impact of drugs on hiPSC-CM contractility.

Within this context, a public-private partnership "InPulse CRACK-IT Challenge" was established between the pharmaceutical company, GlaxoSmithKline (GSK), and a U.K. funding agency, the National Centre for the Replacement, Refinement & Reduction of Animals in Research (NC3Rs). The aim was to develop medium-throughput technology platform that could measure contractility in hiPSC-CMs as a physiologically relevant functional output for use in preclinical drug safety evaluation. Parallel or simultaneous measures for Ca2+ handling and/or voltage, potentially with physiological loading, were requested as part of the challenge as optional parameters to multiplex mechanistically relevant endpoints and thereby inform integrated decision making.

To this end, we established a multinational consortium, comprising 4 academic teams in Germany, Holland, and the United Kingdom, along with 2 biotech companies (Clyde Biosciences; Ncardia), GSK and NC3Rs. We describe the process by which 36 drugs were selected, distributed, and formulated, allowing a training set of 8 drugs to be used to unify standard operating procedures (SOPs). This enabled a multicenter study to be undertaken for blinded evaluation of up to 28 drugs with known positive, negative, or neutral inotropic effects, and led to the creation of an interactive web tool to access datasets for contractility, voltage, and/or Ca2+ handling (https://bjvanmeer.shinyapps.io/crackit/). Overall, the different platform-cell combinations had an accuracy of 44%–85% in correctly predicting inotropy. With simple refinement of the test conditions, namely by adopting approaches to reduce signal-to-noise ratio, data variability, reduce spontaneous beat rate to ≤ 1 Hz, and/or enable chronic testing, accuracy could be increased to 85%–93%, comparing favorably with that currently possible with *in vivo* animal models.

Materials and methods

CellOPTIQ: adult rabbit ventricular cardiomyocytes

Rabbit hearts were excised via a thoracotomy and submerged in a modified Krebs-Henseleit (KH) solution of the following composition (mmol/L): NaCl (130), KCl (4.5), HEPES (5), NaH_2PO_4 (0.4), $MgCl_2$ (3.5), and Glucose (10), pH 7.25 at 37°C with NaOH. Hearts were removed and perfused retrogradely at 25 mL/min (37°C) with a modified KH solution containing 0.75 mmol/L [Ca^{2+}] for 5 min, followed by a nominally Ca^{2+}-free KH solution with 0.1 mmol/L EGTA for 5 min. Hearts were then perfused with KH solution containing 0.24 mmol/L [Ca^{2+}], 1 mg/mL collagenase (type I), and 0.06 mg/mL protease (type XIV). After approximately 4–5 min, enzyme was removed and the left ventricular free wall was then cut into strips in the recirculated enzyme solution containing 1% bovine serum albumin before being mixed to yield a single cell suspension. Cells were maintained in either Ca^{2+}-free KH solution or 1 mmol/L Ca^{2+} (via stepwise increments) until use. Intact cardiomyocytes in 1.8 mmol/L modified Ca^{2+} KH solution were loaded with FluoVolt (Thermo Fisher Scientific) at 1:3000 dilution for 10 min. The incubation medium was removed and the cells resuspended in a modified KH solution.

Cardiomyocytes were allowed to settle on a coverslip in a bath (35 mm petri-dish) at

37°C. Cells were field stimulated at a frequency of 2 Hz with 2 ms duration voltage pulses delivered to parallel graphite electrodes (stimulation voltage set to 1.5 times the threshold) for 2 min before sampling FluoVolt and cell video for 10 s. After repeating this for 10–12 cells/dish the drug was added to quiescent cells and left for 30 min before returning to the same myocytes and repeating the stimulus and data capture protocol. A parallel set of vehicle (DMSO) time control experiments were also performed FluoVolt fluorescence (490 nm excitation) was measured at a sampling rate of 10 KHz, whereas the image was recorded on a CCD camera at 100 Hz frame rate using > 700 nm light. Sarcomere length and fractional shortening of sarcomere length was subsequently extracted from the image using a FFT-based algorithm.

TTM system

The TTM system was developed and used as described previously[16]. Briefly, the all-optical fluorescent system consists of a microscope capable of recording sequential frames while switching exposure wavelengths within 1 ms. Using 3 LEDs at 470, 560, and 656 nm this results in an effective recording speed of 333 Hz per parameter. Baselines measurements (7- s recordings) were made by choosing 3 areas per well and saving the positions to measure the same areas after drug incubation. Data were analyzed with custom software offline and automatically to reduce used bias.

Black glass-bottom 96-well plates (Grenier) were coated with 1:100 Matrigel (Sigma-Aldrich) in DMEM F12 (Sigma-Aldrich). Pluricyte hiPSC-CMs were thawed and plated (40 000/well in 100 µL) according to manufacturer's instructions in Pluricyte Cardiomyocyte Medium. To help the recovery of the cells 1:100 RevitaCell (Sigma-Aldrich) was added to each well. Empty wells around the plated CM were filled with 200 µL of PBS to minimize evaporation. Cells were refreshed with 200 µL Pluricyte medium (PCM) at day 1 and day 4 or 5 after plating. All measurements for 1 drug were always performed on days 5 and 6 or days 6 and 7 after plating.

hiPSC-CMs were labeled with ANNINE 6-plus (Sensitive Farbstoffe GbR, Germany; stock concentration: 0.7 mM, dilution 1:833), Rhod 3 (Invitrogen; stock concentration 10 mM, dilution 1:833), and CellMask Deep Red (Thermo Fisher Scientific; stock concentration 5 mg/mL, dilution 1:1000) in 50 mL PCM for 20 min at 37°C, refreshed (200 mL PCM), and given 10 min to recover at 37°C before recording baseline measurements. Drug incubation took place just after baseline measurements by removing 100 µL medium and adding 100 µL drug solution (30 min at 37°C) prepared according to formulation instructions supplied by GSK.

CellOPTIQ: hiPSC-CMs

The hiPSC-CMs used were R-PAT (derived and differentiated in house as described previously)[17,18], and iCell2 and Pluricyte (purchased from Cellular Dynamics International and Ncardia). Manufacturer instructions were followed for the commercial hiPSC lines. For iCell2, seeding was at 25 000 cells into each well of 96-well plates (Nunclon Delta Surface; Thermo, 167008) and then maintained for 10 days before use in drug evaluation studies. The same plates were used for R-PAT hiPSC-CMs, which were seeded at 40 000 cells/well and maintained until days 20 and 21 of differentiation before use. For Pluricyte hiPSC-CMs, seeding was at 35 000 cells into each well of 96-well plates (Greiner Bio-

One; 655087) and then maintained for 8 days before use. Confluent monolayers of R-PAT and iCell2 hiPSC-CMs were changed into serum-free medium (SFM) (Dulbecco's Modified Eagle Medium [Gibco, 21969035] + 10 mM galactose [Sigma-Aldrich, G0750] and 1 mM sodium pyruvate [Sigma-Aldrich, P2256] 24 h before testing). Pluricyte hiPSC-CMs were changed into 50% SFM and 50% PCM (serum-free) 24 h before day of testing, and on the day of testing were changed into SFM. For the refined conditions described for R-PAT hiPSC-CMs, plating and maintenance were as before but cells were received fresh RPMI-B27 medium 24 h before testing instead of SFM.

hiPSC-CMs in 96-well plate were transiently loaded in 50 µL/well of SFM containing FluoVolt (1:200 part B, 1:2000 part A; Life Tech, F10488) for 20 min at 37°C and 5% CO_2. After incubation, the medium was replaced with 200 µL/well of SFM. Plates were then incubated at 37 °C and 5% CO_2 for 15 min before recording, which were made using a ×40 (NAO.6) objective at 10 kHz. To apply electric field stimulation, a custom-made 8 channel electrode StimStrip (Clyde Biosciences Ltd) was placed in a row of a 96-well plate and connected externally to a box (DC power supply; Lavota). hiPSC-CMs were paced at a frequency of 1.2–1.7 Hz (or 0.7–1 Hz in the refined conditions) with an amplitude of 8 V and a pulse width of 20 ms. Recordings of 10 s were made for each well (contractility was 100 frames/s, hence 1000 frames). Baselines and drug addition were as described for the TTM system. Electrophysiology data were analyzed using CellOPTIQ proprietary software of Clyde Biosciences and were normalized to a maximum amplitude of 1 and minimum of 0 to standardize height for comparison of traces created in OriginPro (OriginLab version 7.5). Contractility data were analyzed based on pixel displacement using an ImageJ plug-in. This plug-in uses a sum of absolute differences algorithm.

Engineered heart tissues

To generate EHTs, in-house hiPSC lines, R-PAT, and ERC18, were differentiated using 2D-monolayer- (R-PAT) or 3D-embryoid body- (ERC18) protocol and fabricated as recently described[19,17]. In brief, casting molds were generated in 24-well plates with 2% agarose (Invitrogen, 15510-019) and Polytetrafluorethylene (PTFE) spacers (EHT Technologies, C0002). PDMS racks (EHT Technologies, C0001) were placed in the 24-well plates so that pairs of PDMS posts reached into each agarose casting mold. A reconstitution mix was prepared consisting of: 1 × 106 hiPSC-CM; 81.9 µL cardiomyocyte medium; 10 µL Matrigel basement membrane matrix (BD 354234); 5.5 µL 2 × DMEM; 0.1 µL Y-27632 (10 mM; Biorbyt orb60104); 2.5 µL bovine fibrinogen (5 mg/mL; Sigma F4753). Reconstitution mix (97 µL) was mixed with prealiquoted 3 µL thrombin (100 U/mL; Biopur BP11-10-1104) and pipetted into the agarose casting mold. GCAMP6f-lentiviral particles (multiplicity of infection: 0.3, functional titer) were included in the EHT reconstitution mix for Ca^{2+} transient analysis. EHTs started to beat coherently after 10–14 days and were analyzed for contraction and Ca^{2+} transient at ≥ 20 days.

EHTs were transferred from culture medium into preequilibrated (37 °C, 40% O_2, 7% CO_2), modified Tyrode's solution (in mM, 120 NaCl; 22.6 $NaHCO_3$; 5.4 KCl; 5 glucose; 1 $MgCl_2$; 0.4 NaH_2PO_4; 0.6–1 $CaCl_2$; 0.05 Na_2EDTA; 25 HEPES) for R-PAT and into DMEM (Gibco 21068028; in mM, 110 NaCl; 44 $NaHCO_3$; 5 KCl; 25 glucose; 0.8 $MgSO_4$; 0.9 NaH_2PO_4, 0.6–1 $CaCl_2$; 25 HEPES, and vitamins and amino acids) for ERC18 EHTs 40 min before analysis to equilibrate to the testing medium. After equilibration, the cumulative

concentration response curve was started with baseline recording in preequilibrated medium with Ca^{2+} concentration of 0.6–1 mM.

For long-term contractility analysis of sunitinib, hiPSC-CM EHTs were equilibrated to regular cell culture medium without serum (DMEM, Biochrom F0415; penicillin/streptomycin 1% [volume/volume], Gibco 15140; aprotinin 5 µM, Sigma-Aldrich A1153; insulin 1.7 µM, Sigma-Aldrich I9278; glutamine 2000 µM, Gibco 25030-081; triiodothyronine 0.77 nM, European Commission-Joint Research Center IRMM-469; hydrocortisone 137 µM: Sigma-Aldrich H0888). Medium change, drug addition and video-optical contractility analysis was performed daily and contraction data was normalized to time control.

Contractility analysis was via automated video-optical contractility analysis was performed in 24-well cell culture plates (Nunc, 122475)[19]. Video files of EHT contractions were analyzed by automated EHT figure recognition software (EHT Technologies, A0001). Top and bottom ends of EHT contour were identified and followed during the course of recording. Force was calculated based on shortening during contraction, elastic propensity, and geometry of PDMS posts.

Ca^{2+} transient analysis was combined with contraction in 24-well cell imaging plates (Eppendorf, 030741005). Briefly, set up consisted of an inverted fluorescence microscope (Zeiss) with a custom-made, automated, light tight, CO_2- and temperature-controlled XY-stage with 24-well plate holder. A camera attached to front port of the microscope was used for contraction analysis (×1.25 objective) and a camera attached to side port of the microscope was used to adjust position of the tissue for fluorescence/Ca^{2+} transient measurement (×10 objective). A small predefined area (0.1 × 0.4 mm) in the center of EHT was used to record Ca^{2+} transients. Mercury lamp, GFP filter set, and photomultiplier tube were used to record change in fluorescence in EHTs expressing GCaMP6f (increase fluorescence during contraction phase). Predefined XYZ coordinates for contraction and Ca^{2+} transient were defined and saved in a bespoke software which controlled microscope settings, XYZ coordinates, and recorded automated-, sequential-contraction and Ca^{2+} transients. Cumulative concentration response curves were performed, similar to contractility analysis, for selective concentrations based on results of contractility analysis.

Data were normalized to a pool of time-matched controls (contractility analysis, ERC18: n = 22 EHTs/7.0 experiments; R-PAT: 16 EHTs/5.0 experiments; combined contractility- and Ca^{2+} transient-analysis: 21 EHTs/8.0 experiments) used for all contractility/combined contractility- and Ca^{2+} transient-measurements. Data are plotted as relative change to the mean baseline, normalized to pool time control. Statistical significance was evaluated by GraphPad Software, 1-way ANOVA with Dunnett's multiple comparisons test versus baseline.

Web tool

The web tool was build using the "Shiny" package in R Language and Environment for Statistical Computing. Data were analyzed and visualized using the packages "ggplot2," "reshape," "Rfast," "ggpubr," "RColorBrewer," "multcomp," and "tidyverse."

Results

Rationale for selection, handling, and distribution of training and blinded drug sets
Driven by the interests of the pharmaceutical industry, and specifically GSK, the 36 drugs in this study (Supplementary Table 1) were selected on basis of: (1) commercial availability; (2) approximate balance in numbers between positive inotropes (PIs), negative inotropes (NIs), and no effect drugs (NE), with respect to contractility; (3) inclusion of false positives or negatives; (4) availability of functional data on inotropic effect on cardiomyocyte and/or heart function from 1 or more species, including human, spanning use *in vitro*, *ex vivo*, preclinically, and clinically; (5) data on free therapeutic plasma concentrations (FTPCs); (6) solubility in DMSO to allow unified testing at a maximum concentration of 0.1% v/v, which does not cause toxicity in hiPSC-CMs; and (7) broad range of modes of action relevant to contractility and toxicity, including modulation of ion channels and pumps in the cell membrane (INaV1.5, IKr, IKATP, ICaL, If, NCX, Na^+/K^+-ATPase) or sarcoplasmic reticulum (SR) (RYR, SERCA), β1- and β2-adrenoceptors, Ca^{2+} sensitivity, signaling cascades (phosphodiesterase [PDE], adenylyl cyclase, cyclic AMP), energy production (ATP, mitochondrial stress), myofilament response, and myofilaments as well as less well-known mechanisms (eg, inhibition of tyrosine kinases).

All drugs were purchased, formulated and distributed under contractual material transfer agreement by GSK to ensure that the same lot numbers were used by the testing laboratories. Eight drugs were not blinded and used as a "training set" to establish the working parameters and protocols for the technology platforms (isoprenaline, nifedipine, digoxin, Bay K 8644, EMD-57033, ryanodine, thapsigargin, caffeine). The remaining 28 "test set" drugs were encoded and blinded by GSK's Sample Management Technology department, which dealt with handling and distribution as preweighed lots in coded brown glass vials. Samples were formulated according to prescribed, blinded instructions, and using single-shot vials of DMSO where possible to minimize absorption of water from the atmosphere, hence avoid inadvertent drug dilution. Powders and formulated drugs were stored at −80°C, with the solutions undergoing no more than 2 rounds of freeze-thaw and use within 2 weeks.

Refining and establishing working parameters with the drug "Training Set"
The training set of 8 drugs was used to unify the methods for testing, analysis, and presentation (Supplementary Figures 1–3). This helped to establish SOPs (Supplementary Table 2), which were used for subsequent blinded evaluation of the "test set" drugs. Three technology platforms were used, differing in configuration, format of wells, and approach to calculate contractility. These were the Triple Transient Measurement (TTM), CellOPTIQ (CO), and engineered heart tissue (EHT) platforms.

The TTM platform is bespoke and was the only system in this study that could simultaneously measure contractility, electrophysiology, and Ca^{2+} handling. Interlaced 1000 frame/s movies (i.e. sequential 1 ms/channel) were recorded from hiPSC-CMs cultured in 2D monolayers in 96-well plates loaded with appropriate dye[20,16]. The CO is a proprietary system that was used to measure contractility, via bright field images, and electrophysiology, via voltage-sensitive dyes[21]. Here, it was used on hiPSC-CMs

cultured in 2D monolayers in 96-well plates and isolated adult rabbit cardiomyocytes. Finally, the EHT system is commercially available, using 3D constructs fabricated from hiPSC-CMs using a fibrin hydrogel between 2 polydimethylsiloxane (PDMS) posts and multiplexed in 24-well plates[22]. Determining Ca^{2+} handling required viral transgenesis of a genetically encoded calcium indicator (GCAMP6f) during EHT fabrication. Whereas pixel displacement was used as a surrogate of contractility in the 2D systems (TTM and CO), 3D EHTs enable force of contraction to be calculated from the extent of deflection of PDMS posts upon each beat.

Action potential duration (APD30, APD90) and triangulation (APD90–APD30) were calculated from voltage waveforms to determine whether electrophysiology was altered, including the appearance of arrhythmias. For Ca2+ handling, amplitude, time to peak, and decay time were assessed, whereas similar parameters (contraction amplitude [CA], contraction time [CT], and relaxation time [RT]) were derived for contraction (Supplementary Figure 2). Contractility responses were further subdivided (Supplementary Figure 2), such that positive inotropy reflected an increase in CA, positive clinotropy a decrease in CT and positive lusitropy a decrease in RT. The opposite is true for negative responses.

The training set of 8 drugs was used to test and refine protocols. Representative data are shown for the PIs, digoxin/isoprenaline, and the NI, nifedipine (Supplementary Figure 3). For each parameter, the percentage change in drug-treated samples relative to their respective vehicle control was calculated using the formula ([drug/drug baseline]/[vehicle/vehicle baseline])*100–100. Consistent with the mode of action of these drugs, in all cases there was a trend or significant response for positive inotropy (increased CA) in hiPSC-CMs treated with digoxin/isoprenaline but negative inotropy (decreased CA) for those treated with nifedipine (Supplementary Figure 3). Digoxin tended to increase RT in 2D configuration, whereas isoprenaline decreased of both CT and RT in 3D EHTs (Supplementary Figure 3). These studies allowed unification of SOPs, although physical and technical constraints between the platforms meant that some unavoidable differences remained (Supplementary Table 2).

Blinded evaluation and assignment of drug "Test Set"

Using the SOPs established above, up to 28 blinded drugs were tested in a rank order that was predefined by GSK (Table 1). Contraction was the parameter common to all platforms because the primary aim of the study was to predict whether drugs were positive, negative, or neutral inotropes. Differentiation of the in-house hiPSC lines, R-PAT, and ERC18, provided sufficient hiPSC-CMs to test all available drugs on the CO and/or EHT platforms. Testing was restricted to 10 drugs in rabbit CMs (as a comparator) and in commercial hiPSC-CMs (Pluricyte and iCell2) due to cost, availability and timelines, whereas throughput was a limitation of the TTM system. Overall, 9 drugs were tested in common across all platform-cell combinations, which were later unblinded and identified as: PIs, epinephrine, forskolin, levosimendan, pimobendan; NIs, verapamil, sunitinib; NE, acetylsalicylic acid, atenolol, captopril.

All data for contraction, voltage, and Ca^{2+} handling across the various platform-cell combinations are accessible via an interactive web tool via https://bjvanmeer.shinyapps.

io/crackit/. Representative data for contractility illustrates the output format for 6 drugs where the response was generally predicted correctly or incorrectly, respectively. Thus, data are shown for the PIs, epinephrine, and levosimendan (Figure 1A), NIs, verapamil, and sunitinib (Figure 1B), and NE drugs, acetylsalicylic acid, and captopril (Figure 1C). In some instances, data from Ca^{2+} and, to a lesser extent, voltage analyses were used to assist in prediction of inotropic response, as was the case for the PI, epinephrine, and the NI, verapamil (Supplementary Figures 4A and 4B).

Prediction of inotropy involved a 2-day face-to-face meeting between all investigators, with colleagues from GSK overseeing the process as observers rather than contributors. Each platform-cell-drug combination was evaluated individually and a consensus between the research team on the outcome was established using the terminology defined in Supplementary Figure 2 (i.e. positive or negative inotropy [CA], clinotropy [CT], and lusitropy [RT]; altered electrophysiology ± arrhythmias [AE ± *]; altered Ca^{2+}). In some cases, decisions were based on trends rather than statistical significance. For example, this was true for TTM: Pluricyte evaluation of epinephrine (Figure 1A, see CA and CT). Once predictions were finalized, the document was "locked" and drugs were unblinded by GSK to allow comparison with their known effects (Tables 1 and 2).

Across the 9 drugs evaluated in common, all platforms mainly predicted NE drugs and NIs (Table 2). One exception was sunitinib, which was poorly detected by the EHT platform. This may be due to slower penetration, lower sensitivity, and greater cell community effect of 3D tissues protecting against short-term (30 min) exposure to this chronic toxicant. Poorest predictivity was for PIs, which ranged from 0% to 50% accuracy. Overall predictivity for the 9 drugs ranged from 44% to 78%. This range was similar across all drugs tested (50%–85%), with NE and NI being predicted most accurately (up to 100%; Table 2). The trend was for the EHT:hiPSC-CM combination to be more predictive of PIs (75%) than CO: hiPSC-CM (0%–25%). Together, these data implied that continuous measurements from 3D preparations of hiPSC-CMs yielded more predictive contractility data than cell motion sampled from a 2D culture.

We looked for trends in the data that might point toward ways to improve the process of predicting response. The drug concentration at which the maximum responses were recorded were broadly similar across the TTM, CO, and EHT platforms, irrespective of whether prediction was correct (Table 1). However, we noted that the response range was wider in 2D relative to 3D platforms. Whereas mean maximum measurable percentage changes in CA for the TTM and CO platforms ranged from –100% to +196%, it was –100 to +53% for the EHT platform (Table 1). Where there was an increase in CA, the standard deviation of these mean values was 41.5 versus 12.1 for the 2D versus 3D platforms. A similar pattern was observed for NIs, and for changes in CT and RT. This was corroborated by the wider distribution of data points in the 2D platforms relative to the 3D platform (Figures 1A-C, Supplementary Figures 4A and 4B, web tool). This likely relates in part to the cumulative concentration response protocol used for EHTs (Supplementary Table 2).

These observations prompted us to examine sensitivity of the different platforms. Where platform-cell combinations correctly predicted inotropy, data were converted

A

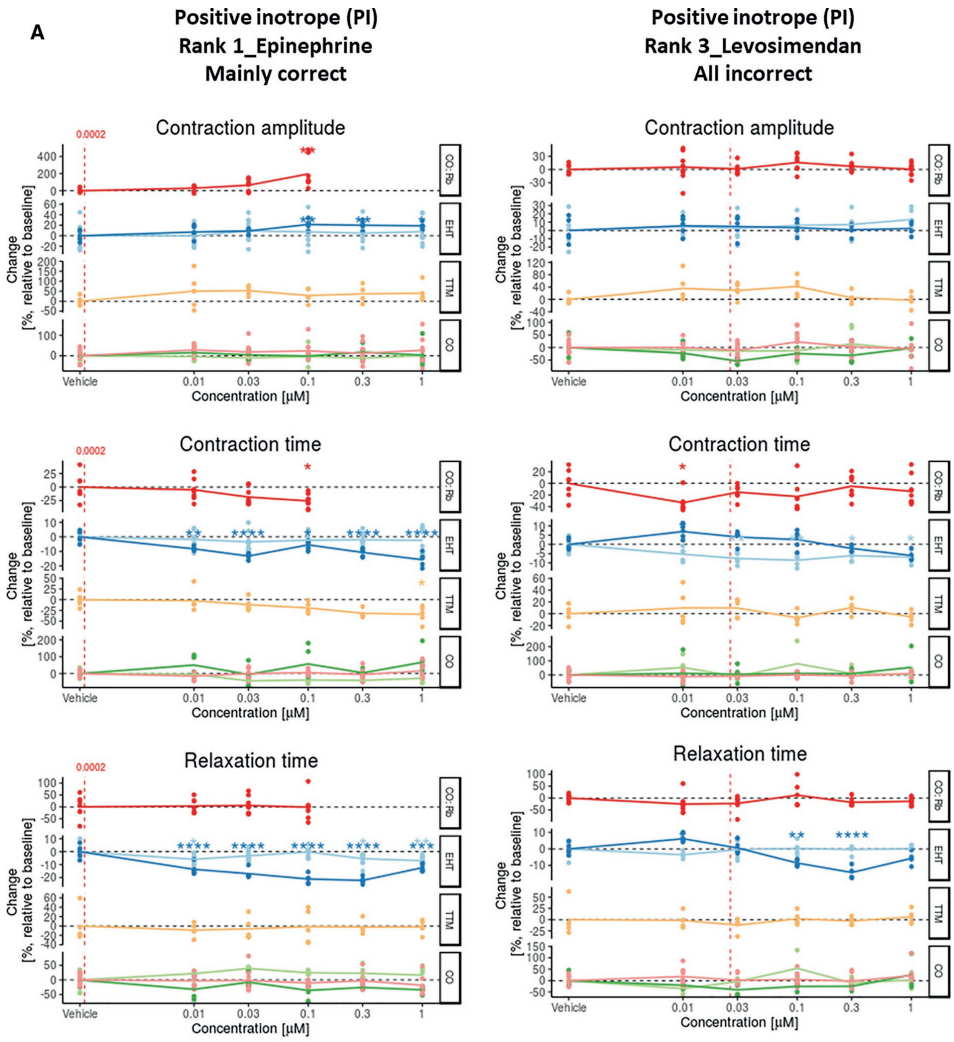

	Predicted correctly? Epinephrine	Predicted correctly? Levosimendan
CO: Rb: Rabbit CMs	Yes	No
EHT: R-PAT	Yes	No
EHT: ERC	No	No
TTM: Pluricyte	Yes (with Ca^{2+})	No
CO: R-PAT	No	No
CO: iCell2	Yes	No
CO: Pluricyte	No	No

into a heat map to reflect the percentage change for NIs (Figure 2A) and PIs (Figure 2B). In 6/7 correctly predicted cardio-active PIs, 1 or more contractile parameters (CA, CT, and/or RT) recorded from EHTs reached statistical significance at concentrations within, or close to, the FTPC range, whereas 2D platforms appeared to be less sensitive (Figure 2B). This is illustrated by epinephrine, where significant changes (p of ≤ 0.05, Dunnett's post-test) in CT and RT were detected within the FTPC range at a sensitivity of 10- to 100-fold greater than the 2D platforms, and a similar pattern was seen for forskolin (Figure 2B). These trends did not extend to NIs, presumably because on- or off-target cardiac toxicity associated with a proportion of compounds in this group will be occurring after longer incubation times and at higher concentrations than those used for therapeutic benefit, which is reflected in the FTPC.

Finally, we investigated which parameter was most informative (Figure 3). Where prediction was correct, we asked which parameter within these *in vitro* models reached significance at the lowest drug concentration. Pooled data from both PIs and NIs showed no clear distinction between CA, CT, and RT. However, segregation showed that CA was clearly most informative parameter for NIs. In contrast, CT was highly informative for PIs and particularly those with cAMP-mediated modes of action, with some contribution being derived from RT in hiPSC-CMs and CA in rabbit CMs.

Understanding why incorrect assignments were made and improving test platforms
The data above highlighted several deficiencies, including: (1) the discrimination of changes in contractility assessed from intermittent video measurements using a motion algorithm on 2D systems was lower than the continuous tension measurements on

Figure 1: Contraction analysis across the platform-cell combinations for PIs and NIs.

A, Contraction analysis across the platform-cell combinations for PIs. Examples are given to illustrate when some or all platform-cell combinations enable correct or incorrect predictions of the PIs, epinephrine, and levosimendan, respectively. The table indicates where decision making was guided by data from Ca^{2+} transients and/or voltage, with example data provided for epinephrine and verapamil in Supplementary Figures 4A and 4B. B, Contraction analysis across the platform-cell combinations for NIs. Examples are given to illustrate when some or all platform-cell combinations enable correct or incorrect predictions of the NIs, verapamil, and sunitinib, respectively. The table indicates where decision making was guided by data from Ca^{2+} transients and/or voltage, with example data provided for epinephrine and verapamil in Supplementary Figures 4A and 4B. C, Contraction analysis across the platform-cell combinations for NEs. Examples are given to illustrate when some or all platform-cell combinations enable correct or incorrect predictions of the NEs, acetylsalicylic acid, and captopril, respectively.

Red dotted line is free therapeutic plasma concentration (FTPC). Dunnett's stats versus vehicle control: *p < 0.05; **p < 0.01; ***p < 0.001; ****p < 0.0001. Abbreviations: CO, CellOPTIQ; EHT, engineered heart tissue; TTM, Triple Transient Measurement.

A

Drug	Rank	CellLine	parameter	Concentration 0.01	0.03	0.1	0.3	1	3	10	30	100
Verapamil	7		FTPC		0.05 µM							
		CO: Rb	CA	-54.95	-82.09	-80.27	NR	NR				
			CT	-7.87	-7.92	24.26	NR	NR				
			RT	15.17	23.28	60.89	NR	NR				
		EHT: ERC	CA	-8.17	-42.18	-89.19	-100	-100				
			CT	-1.06	-9.48	-25.36	NR	NR				
			RT	-10.05	-17.26	-16.33	NR	NR				
		EHT: R-PAT	CA	5.93	-26.48	-100	-100	NR				
			CT	3.79	-7.32	NR	NR	NR				
			RT	4.07	-6.23	NR	NR	NR	-	-	-	-
		TTM:	CA	-30.53	-50.11	-78.76	NR	NR	-	-	-	-
			CT	-11.49	-31.01	-68.09	NR	NR	-	-	-	-
			RT	-0.44	-8.95	-11.2	NR	NR	-	-	-	-
		CO: iCell2	CA	36.23	-7.03	8.1	-39.6	-100	-	-	-	-
			CT	103.13	84.97	4.58	-7.93	-100	-	-	-	-
			RT	31.3	4.47	47.12	-10.27	-100	-	-	-	-
		CO: Pluricyte	CA	30.6	-6	24.3	8.3	-100	-	-	-	-
			CT	3.43	18.5	-11.54	-41.46	-100	-	-	-	-
			RT	-35.77	-32.36	-60.72	-59.18	-100	-	-	-	-
		CO: R-PAT	CA	12.04	3.47	-11.34	-26.84	-98.03	-	-	-	-
			CT	-35.26	-16.5	-16.76	-36.58	-80.63	-	-	-	-
			RT	-5.87	1.28	14.88	-25.46	-87.94	-	-	-	-
Sunitinib	9		FTPC	0.003 µM								
		CO: Rb	CA	-	-	17.79	7.28	-31.96	-57.64	-77.7	-	-
			CT	-	-	4.17	-2.68	3.91	5.18	45.93	-	-
			RT	-	-	8.87	0.33	23.64	137.67	300.4	-	-
		TTM:	CA	-	-	42.31	27.59	15.24	-39.48	-20.73	-	-
			CT	-	-	9.95	13.19	-4.28	-17.53	-23.25	-	-
			RT	-	-	28.32	19.51	22.97	18.57	9.33	-	-
		CO: iCell2	CA	-	-	7.6	-16.86	-20.5	4.82	-24.76	-	-
			CT	-	-	-11.92	11.7	-43.4	-11.72	9.86	-	-
			RT	-	-	1.78	-2.26	62.3	5.38	-7.1	-	-
		CO: Pluricyte	CA	-	-	-13.02	4.46	3.08	17.57	-100	-	-
			CT	-	-	162.66	58.3	16.26	24.83	-100	-	-
			RT	-	-	-46.48	-1.14	-10.16	-19.22	-100	-	-
Citalopram	16		FTPC		0.05 µM							
		EHT: ERC	CA	-	-	-	-	-26.58	-65.22	-100	-100	-100
			CT	-	-	-	-	1.82	0.76	NR	NR	NR
			RT	-	-	-	-	5	7.72	NR	NR	NR
		EHT: R-PAT	CA	-	-	-	-	-1.52	-30.72	-100	NR	NR
			CT	-	-	-	-	6.49	-4.03	NR	NR	NR
			RT	-	-	-	-	4.96	-1.33	NR	NR	NR
		CO: R-PAT	CA	-	-	-	-	11.74	-13.54	-61.3	-100	-100
			CT	-	-	-	-	-11.44	-2.23	-19.46	-100	-100
			RT	-	-	-	-	6.18	-8.13	-30.71	-100	-100
Itraconazole	18		FTPC	0.00086 µM								
		EHT: ERC	CA	-	-	-9.9	-16.06	-36.58	-51.18	-100	-	-
			CT	-	-	6.88	6.19	11.31	8.49	NR	-	-
			RT	-	-	1.93	1.74	-10.18	-29.37	NR	-	-
		EHT: R-PAT	CA	-	-	5.93	-1.39	-15.86	-51.14	NR	-	-
			CT	-	-	13.55	4.63	4.61	12.2	NR	-	-
			RT	-	-	-2.65	-8.52	-19.46	-33.17	NR	-	-
		CO: R-PAT	CA	-	-	-32.83	-25.86	-16.36	-48.12	-100	-	-
			CT	-	-	8.5	25.46	6.66	-29.86	-100	-	-
			RT	-	-	-2.15	-2.14	-2.08	-62.62	-100	-	-
Sorafenib	19		FTPC		0.03 µM							
		EHT: ERC	CA	-	-	-15.06	-16.8	-22.49	-37.56	-56.3	-	-
			CT	-	-	-1.34	-2.42	3.62	6.27	4.68	-	-
			RT	-	-	3.4	2.78	-1.17	-14.39	-24.43	-	-
		EHT: R-PAT	CA	-	-	-1.68	-3.89	-11.75	-25.63	-50.4	-	-
			CT	-	-	3.22	1.8	8.7	6.42	13.89	-	-
			RT	-	-	0.22	1.31	-1.98	-6.48	1.55	-	-
		CO: R-PAT	CA	-	-	-12.8	-2.87	-10.56	-49.21	-100	-	-
			CT	-	-	4.36	28.21	10.03	-48.43	-100	-	-
			RT	-	-	-3.54	23.61	-12.26	-55.88	-100	-	-
Ivabradine	20		FTPC		0.01 - 0.1 µM							
		EHT: ERC	CA	-	-	-5.9	-7.34	-9.23	-19.14	-55.6	-	-
			CT	-	-	0.77	-0.27	-3.68	-8.35	-13.62	-	-
			RT	-	-	-1.61	-3.04	4.08	27.35	45.3	-	-
		EHT: R-PAT	CA	-	-	-6.21	-7.39	-2.05	8.83	-15.68	-	-
			CT	-	-	0.17	-7.87	-6.8	-13.46	-26.88	-	-
			RT	-	-	3.15	0.06	-1.13	-0.25	-2.34	-	-
Flecainide	22		FTPC			0.2 - 0.4 µM						
		EHT: ERC	CA	-	-	-8.14	-9.09	-24.62	-38.05	-74.5	-	-
			CT	-	-	3.26	-0.71	-4.9	-21.24	NR	-	-
			RT	-	-	0.83	1.07	18.08	42.22	NR	-	-
		EHT: R-PAT	CA	-	-	-5.47	-20	-6.8	-100	NR	-	-
			CT	-	-	-4.73	-15.53	-6.29	NR	NR	-	-
			RT	-	-	-5.29	-17.79	-25.78	NR	NR	-	-
Phentolamine	24		FTPC						2.25 µM			
		EHT: ERC	CA	-	-	-	-	-1.62	-23.21	-89.9	-100	-100
			CT	-	-	-	-	-8.02	-16.4	-30.49	NR	NR
			RT	-	-	-	-	25.36	39.86	52.53	NR	NR
		EHT: R-PAT	CA	-	-	-	-	-3.14	-28.82	NR	NR	NR
			CT	-	-	-	-	-4.82	-17.74	NR	NR	NR
			RT	-	-	-	-	-12.69	-27.78	NR	NR	NR
		CO: R-PAT	CA	-	-	-	-	-20.04	-27.6	-41.1	-100	-100
			CT	-	-	-	-	-7.2	-7.9	-22.32	-100	-100
			RT	-	-	-	-	41.8	-2.7	-23.44	-100	-100
Zimelidine	28		FTPC					0.78 µM				
		EHT: ERC	CA	-	-	-	-	5.12	-6.91	-37.4	-95.23	-100
			CT	-	-	-	-	-3.17	-8.58	-13.03	-24.92	NR
			RT	-	-	-	-	23.76	42.78	42.59	27.92	NR
		EHT: R-PAT	CA	-	-	-	-	18.37	-1.27	NR	NR	NR
			CT	-	-	-	-	-2.11	-15	NR	NR	NR
			RT	-	-	-	-	-7.02	-22.03	NR	NR	NR

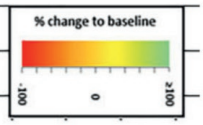

B

Concentration (μM)

Drug	Rank	CellLine	parameter	0.01	0.03	0.1	0.3	1	3	10	30	100
Epinephrine	1		FTPC	0.0002 - 0.05 μM								
		CO: Rb	CA	30.07	65.04	**196.24**	NR	NR				
			CT	-5.19	-18.51	**-25.74**	NR	NR				
			RT	3.81	5.91	-1.28	NR	NR				
		EHT: R-PAT	CA	7.09	9.12	**21.56**	**20.03**	**19.01**				
			CT	**-8.25**	**-13.22**	**-5.5**	**-10.7**	**-15.73**				
			RT	**-13.66**	**-16.98**	**-21.16**	**-22.2**	**-12.31**				
		TTM:	CA	50.36	52.81	28.71	36.91	39.83				
			CT	-2.29	-11.44	-18.99	-31.56	**-33.84**				
			RT	-8.72	-5.98	-1.49	-2.16	-1.96				
		CO: iCell2	CA	-3.6	-10.7	-3.9	-11.66	0.88				
			CT	-4.16	-42.92	-37.92	-39.86	-27.74				
			RT	21.74	39.32	24.58	23.08	16.28				
Forskolin	2		FTPC	0.012 - 0.024 μM								
		CO: Rb	CA	-	-	-12.35	13.09	-4.22	-15.54	7.04	-	-
			CT	-	-	-33.78	6.68	30.44	-5.28	8.26	-	-
			RT	-	-	7.1	9.92	36.35	45.43	34.6	-	-
		EHT: ERC	CA	-	-	-3.31	3.37	15.59	17.71	13.29	-	-
			CT	-	-	**-23.21**	**-30.5**	**-32.53**	**-30.3**	**-32.7**	-	-
			RT	-	-	**-11.15**	**-13**	**-18.03**	**-22.4**	**-23.2**	-	-
		EHT: R-PAT	CA	-	-	5.07	3.93	9.63	-0.39	-15.07	-	-
			CT	-	-	-2.05	**-7.33**	2.09	-0.56	-4.19	-	-
			RT	-	-	-3.69	**-17.1**	**-20.9**	**-21.8**	**-19**	-	-
		TTM:	CA	-	-	31.98	22.85	6.31	13.63	7.17	-	-
			CT	-	-	-26.83	-26.78	**-31.31**	**-37.4**	**-35.1**	-	-
			RT	-	-	11.15	-38.03	-37.12	-28.9	-33.23	-	-
Pimobendan	4		FTPC	0.005 - 0.01 μM								
		EHT: ERC	CA	-	-	-	-	-3.26	-7.67	5.58	13.42	13.29
			CT	-	-	-	-	-9.17	**-12.5**	**-11.2**	-8.21	**-11.4**
			RT	-	-	-	-	-3.72	3.43	5	13.03	13.55
Dobutamine	11		FTPC			0.07 - 1 μM						
		EHT: ERC	CA	-	-	5.01	3.75	**17.2**	**18.07**	12.27	-	-
			CT	-	-	-2.43	**-11.5**	**-26.23**	**-31.7**	**-37.2**	-	-
			RT	-	-	1.97	7.23	-4.42	-6.38	1.23	-	-
		EHT: R-PAT	CA	-	-	**17**	**28.48**	**37.5**	**43.62**	**31.95**	-	-
			CT	-	-	**-9.74**	**-12.9**	**-11.53**	**-12.3**	**-25.2**	-	-
			RT	-	-	**-20**	**-20.3**	**-18.29**	**-17.9**	**-21.6**	-	-
Milrinone	13		FTPC			0.1 - 0.15 μM						
		EHT: ERC	CA	-	-	-	-	2.32	1.61	-0.59	7.51	7.64
			CT	-	-	-	-	**-7.84**	**-8.45**	**-12.9**	**-15.57**	**-17.6**
			RT	-	-	-	-	2.96	0.11	0.33	-6.06	-1.51
		EHT: R-PAT	CA	-	-	-	-	-1.98	-2.27	4.87	18.46	NR
			CT	-	-	-	-	0.4	-5.11	-1.59	-10.85	NR
			RT	-	-	-	-	-0.07	-2.91	-3.65	**-8.98**	NR
Omecamtiv mecarbil	14		FTPC		0.05 - 0.42 μM							
		EHT: ERC	CA	3.03	5.86	11.22	**20.63**	**21.75**	-	-	-	-
			CT	0.66	0.04	3.8	18.9	37.51	-	-	-	-
			RT	2.88	1.98	-1.06	-5.53	-1.94	-	-	-	-
		EHT: R-PAT	CA	-12.48	0.75	17.48	**53.19**	NR	-	-	-	-
			CT	-2.22	2.07	**19.04**	**36.85**	NR	-	-	-	-
			RT	1.43	1.17	-9.2	**-25.8**	NR	-	-	-	-
Terbutaline	21		FTPC					1.3 μM				
		EHT: ERC	CA	-	-	4.46	9.04	**16.84**	**23.59**	**29.18**	-	-
			CT	-	-	**-22.01**	**-28.4**	**-29.62**	**-23.9**	**-22.3**	-	-
			RT	-	-	-14.96	-16.51	-17.06	-16.25	-1.97	-	-
		EHT: R-PAT	CA	-	-	7.94	1.9	14.3	**17.48**	NR	-	-
			CT	-	-	**-14.82**	**-21.3**	**-16.82**	**-24.2**	NR	-	-
			RT	-	-	**-24.73**	**-35.2**	**-30.03**	**-32.8**	NR	-	-

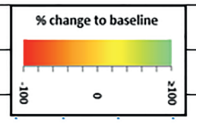

Figure 2: Sensitivity of platform-cell combinations for predicting PIs and NIs.

A, Sensitivity of platforms-cell combinations for predicting negative inotropes (NIs). Where NIs were correctly predicted, data are presented as percent change relative to baseline for any of the 3 contractility parameters (CA, contraction amplitude; CT, contraction time; RT, relaxation time). The bolded black text indicates where significance was reached using Dunnett's stats versus vehicle control and $p < 0.05$. Abbreviations: CO, CellOPTIQ; EHT, engineered heart tissue; FPTC, free plasma therapeutic concentration; NR, not recorded; TTM, Triple Transient Measurement. B, Sensitivity of platform-cell combinations for predicting positive inotrope (PIs). Where PIs were correctly predicted, data are presented as percent change relative to baseline for any of the 3 contractility parameters (CA, contraction amplitude; CT, contraction time; RT, relaxation time). The bolded black text indicates where significance was reached using Dunnett's stats versus vehicle control and $p < 0.05$.

3D systems, (2) detection of PIs was challenging, particularly to 2D platforms, and (3) chronic toxicants, such as doxorubicin, were poorly predicted after the acute (30 min) treatment duration.

We reasoned that medium composition may be a contributing factor in signal-to-noise ratio and poor detection of PIs. This was because, on the CO platform, switching from protein-containing (RPMI-B27) to serum-/protein-free medium increased the mean beat rate from 0.7 to ≥ 1.2 Hz (Supplementary Figure 5; $p \leq .0001$, Mann-Whitney). This was concurrent with increased spread of the data for CA, CT, and RT, wherein the standard deviations for RPMI-B27 versus serum-/protein-free medium were 12.1 versus 32.8, 14.5 versus 20.1, and 10.7 versus 26.9, respectively (Supplementary Figure 5). It has previously been reported in native heart muscle preparations that lower beating rate is associated with a positive force-frequency relationship (up to approximately 2 Hz) and stronger inotropic effects of most PIs[23]. Therefore, we retested PIs from the test set of drugs using CO:R-PAT, because this platform:cell combination proved poorly predictive (0/8) in the blinded study. In these revised testing conditions, 6/8 PIs showed reduced CT and/or RT (Figure 4).

We extended these studies to the 3D EHT platform, this time slowing spontaneous beating to < 0.5 Hz with 300 nM ivabradine, a pharmacological blocker of the "funny" If current[24]. Notably, these "slowed" EHTs could faithfully follow electrical pacing in increments from 0.5 to 2.5 Hz (Supplementary Figure 6). Whereas force-frequency relationships was negative above 1.5 Hz, it was positive between 0.5 and 1.5 Hz, evidenced by a 147% increase in force generation concurrent with significant shortening of CT and RT (Supplementary Figure 6). We therefore re-evaluated 6 of the PIs in the presence of 300 nM ivabradine with electrical pacing at 0.5, 0.7, 1.0, 1.5, and 2.0 Hz. These also included epinephrine, levosimendan, and pimobendan, which had been incorrectly predicted by EHT:R-PAT and/or EHT:ERC platform-cell combinations. Notably, for all 6 drugs, positive inotropy was evident via increases in CA but only at 0.5 and 0.7 Hz, and sometimes at 1 Hz, but never at 1.5 or 2 Hz (Figure 5). Consistent with this, shortening of CT was observed for all drugs acting via increased cAMP, with

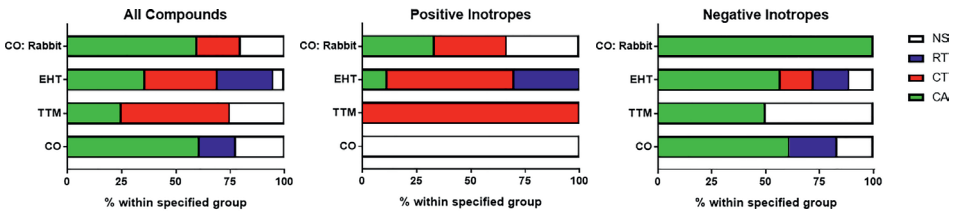

the largest changes often occurring at the lower pacing frequencies (Figure 5). Thus, in both 2D and 3D configurations, lower beating frequencies led to increased predictivity for PIs.

Finally, we considered NIs that had been incorrectly predicted (or not tested), including doxorubicin and sunitinib. Although 30 min exposure of hiPSC-CMs to these anticancer drugs altered electrophysiology, effects on contractility were predicted with variable accuracy (Table 1, web tool). We asked whether longer term exposure would affect contractility (Supplementary Figure 7). The CO:R-PAT platform-cell combination showed that exposure to the highest concentration of either drug for 24 h led to loss of contraction and cell death. Similarly, using the EHT:ERC platform-cell combination, exposure to doxorubicin ceased EHT contraction after 17.5 h, whereas exposure to 1 μM sunitinib led to a decline in CA over a 7-day period (Supplementary Figure 7). Thus, although short-term exposure to these NIs perturbed the electrophysiology of hiPSC-CMs, longer term exposure caused overt cytotoxicity and/or negative inotropy.

Discussion

Through blinded testing across multiple geographical sites, we evaluated the ability of 7 different platform-cell combinations to predict whether drugs of interest to the pharmaceutical industry were positive, negative, or neutral inotropes. We achieved this by examining contractility parameters (CA, CT, and RT), as well as using Ca^{2+} transients and/or electrophysiology to assist in decision making in some instances. Within the context of these *in vitro* models, we found that CA was the most informative parameter for NIs. Particularly after refinement involving slowing of beat rate to below 1 Hz (Figure 5, Supplementary Figure 6), CA was highly informative of PIs in the EHT system but far less so in the 2D systems. Although contraction- and relaxation-time provided confirmatory readouts for PIs in 3D EHTs, these parameters typically served as the primary source of predictivity in 2D (Figure 4), especially where the mode of action involved cAMP signaling.

Figure 3: Most informative contractility marker.

Parameters that led to the correct prediction of drug responses were assessed. Data show the breakdown by percentage for the parameters (CA, contraction amplitude; CT, contraction time; RT, relaxation time) that reached significance at the lowest concentration (Dunnett's stats vs vehicle control and $p < 0.05$). White boxes (NS, not significant) indicate where predictions were made due to a trend rather than reaching significance, and/or by guidance from Ca^{2+} and/or voltage data. Abbreviations: CO, CellOPTIQ; EHT, engineered heart tissue; TTM, Triple Transient Measurement.

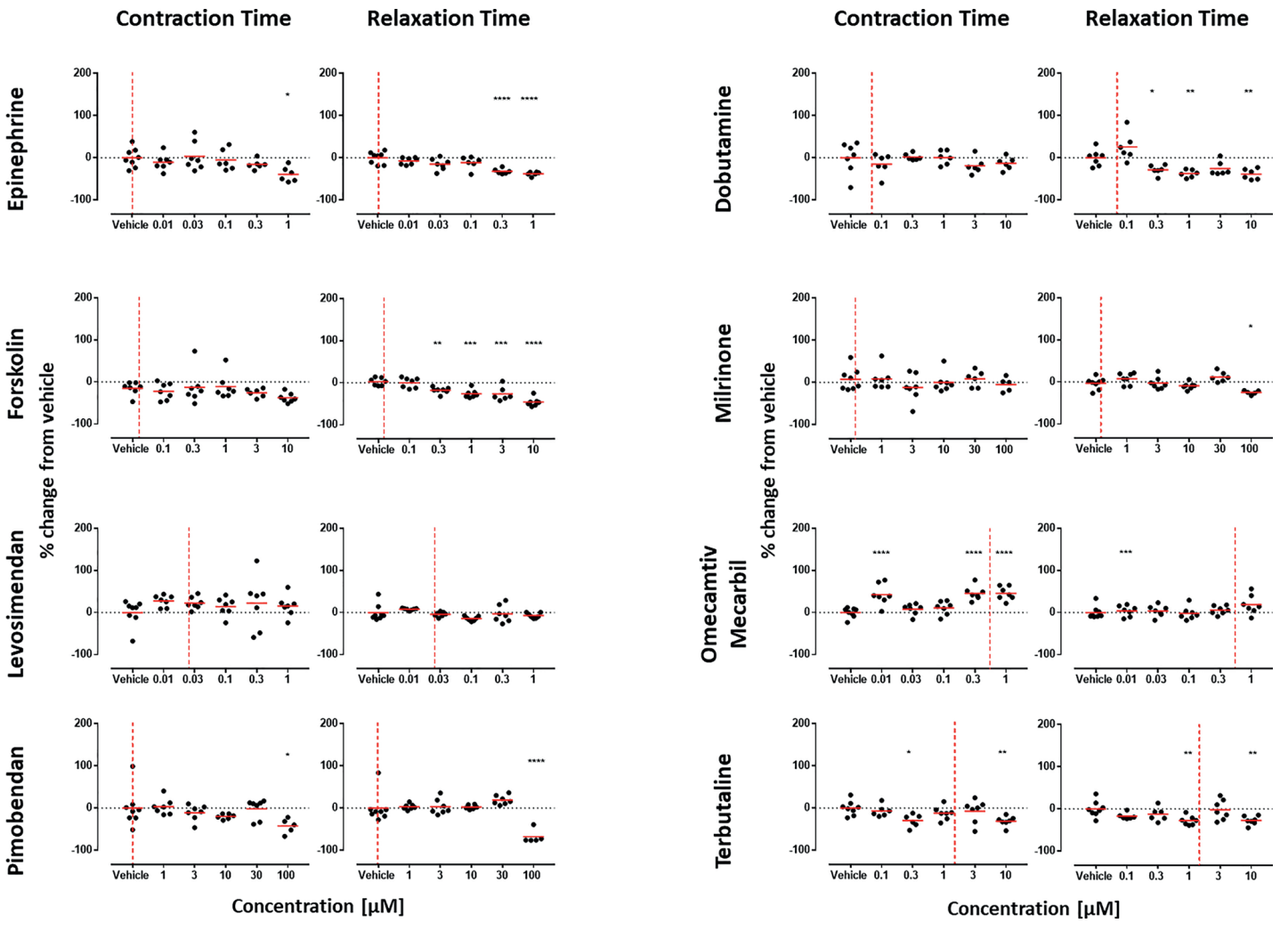
Contraction Time
Relaxation Time
Epinephrine
Forskolin
Levosimendan
Pimobendan
Dobutamine
Milrinone
Omecamtiv Mecarbil
Terbutaline
% change from vehicle
Concentration [µM]

We propose that an efficient way to predict the inotropic effect of drugs would be first to conduct acute (30 min) testing in hiPSC-CMs. Spontaneous beat rates should be < 1 Hz, which can be achieved by modifying the culture medium, using pharmacological blockage with ivabradine, and/or selecting hiPSC-CMs with slow intrinsic rates. In EHTs, this approach unveiled a clear positive force-frequency relationship. If no changes in inotropy are detected in the acute assay, then exposure times can be increased to ≥ 24 h to determine whether the drugs have a chronic effect. These timelines were suggested by GSK (ie, ≤ 30 min considered as acute; ≥ 24 h as chronic), which proved to be a useful approach because it allowed a predictive accuracy of 85% in 2D monolayers and 93% in 3D EHTs.

In reaching these refined conditions, we noted greater importance of the cell preparation protocol, testing conditions, methods of measuring contractility, and 2D versus 3D than the cell type used, which was not necessarily expected. There were differences in the purity/composition of the different cell types and in their baseline electrophysiological characteristics, which partly reflects their maturity state at single cell level (Supplementary Table 3). However, there was not an obvious correlation between these differences and predictivity. For example, initial testing of the same cell type (Pluricyte hiPSC-CMs) on 2 platforms (TTM and CO) gave different accuracies (78% vs 56%). The same was true for R-PAT hiPSC-CMs on the EHT and CO platforms (67% vs 44%).

Modifying both the culture environment (by including a protein source that caused a beat rate to be slowed, and signal-to-noise ratio and data variability to be reduced) and the drug exposure conditions (by including both acute chronic testing for ≤ min and ≥ 24 h, respectively) for the CO:R-PAT combination allowed the accuracy of prediction using this cell line to be increased to 85%. It is possible that further improvements could be made, whilst simultaneously shedding light on mechanism of action. For example, analysis of data during different stages of relaxation identified positive lusitropy for dobutamine (at 50% relaxation) and late relaxation deficit for ivabradine (at 80% relaxation). During the blinded phase, we also correctly predicted that drug rank 14 was omecamtiv mecarbil on account of the unusual response of increased CT (approximately

Figure 4: Refined culture conditions increase predictivity of PIs in 2D monolayers of hiPSC-CMs.

Contraction analysis was carried out on the 8 PIs from the drug test set using the CO:R-PAT platform-cell combination. Only CT and RT are shown because data in Figure 3 showed these to be the most informative parameters for PIs. Whereas testing in serum-/protein-free medium failed to identify any PIs correctly (web tool), the slowed beat rate and improved signal-to-noise ratio afforded by culture in RPMI-B27 allowed correct identification of 6/8 PIs by significant decreases in CT and/or RT. Red dotted line is free therapeutic plasma concentration. Dunnett's stats versus vehicle control: *p <0 .05; **p < 0.01; ***p < 0.001; ****p < 0.0001.

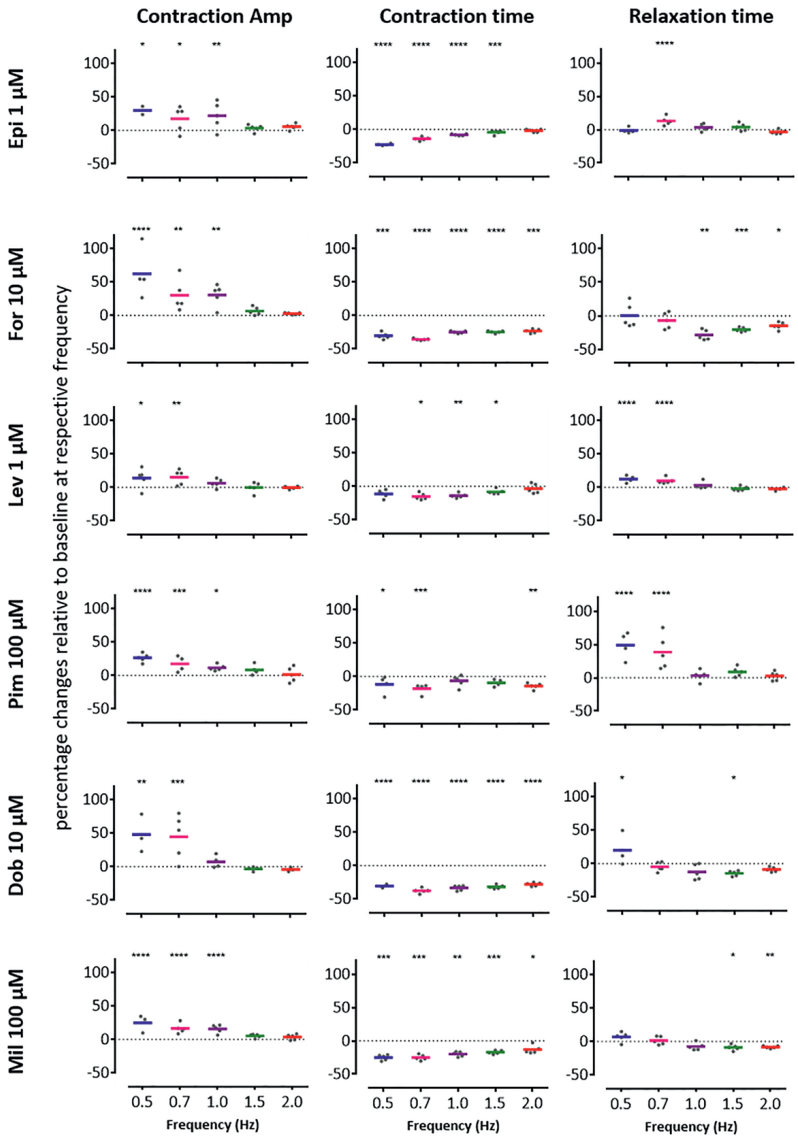

Figure 5: Slowed beat rate increases the predictivity of PIs) in 3D EHTs.

Contraction analysis was carried out using EHTs with 6 of the PIs from the drug test set: epinephrine (Epi), forskolin (For), levosimendan (Lev), pimobendan (Pim), dobutamine (Dob), and milrinone (Mil) which had been predicted with variable accuracy (web tool). In all cases, the drugs (applied as a high concentration bolus) increased contraction amplitude (CA) but only at

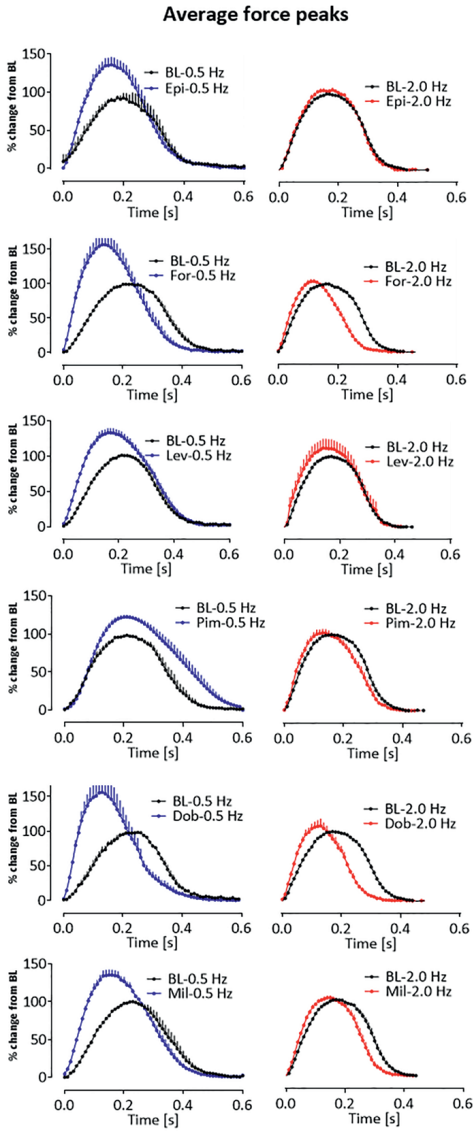

0.5 and 0.7 Hz, and sometimes at 1 Hz, with the largest effects seen in contraction time (CT) also often occurring at these frequencies. Scatter plots show percentage changes relative to baseline at respective frequency. Averaged peaks for force are shown for baseline (BL, black peaks) versus after treatment in EHTs paced at 0.5 Hz (blue peaks) or 2.0 Hz (red peaks). Dunnett's stats versus baseline at respective frequency: *$p < 0.05$; **$p < 0.01$; ***$p < 0.001$; ****$p < 0.0001$.

+40%) without convincing evidence for increased CA[25]. This shows the value of applying pharmacological knowledge to drug responses in hiPSC-CMs to derive mechanistic information out of multiparametric assessments, in this case combined evaluation of CA, CT, and RT in hiPSC-CMs configured as 3D EHTs, in this case combined evaluation of CA, CT, and RT in hiPSC-CMs configured as 3D EHTs.

Another consideration is the difference between single cells, continuous monolayers, and 3D engineered constructs. The single rabbit cardiomyocyte assay used near-physiological rates of stimulation (2 Hz) and subphysiological rates (1 Hz or lower) may have improved scope to detect PIs. In adult heart preparations, a common feature of PI interventions that raise intracellular Ca^{2+} is the occurrence of spontaneous diastolic SR Ca^{2+} release. This phenomenon is linked to negative inotropy and arrhythmic behavior in single cells and intact myocardium[26,27]. In this study, spontaneous diastolic Ca^{2+} release and associated diastolic shortening was observed in isolated rabbit myocytes in response to β-adrenoreceptor stimulation and drugs that raise cAMP directly (e.g. forskolin), but this phenomenon was not reported in any of the hiPSC-CMs platforms. This is consistent with the minimal involvement of the SR in excitation-contraction coupling typically seen in embryonic cardiomyocytes and hiPSC-CMs[28]; in this context, the PI effect from cAMP arises mainly from cAMP-mediated stimulation of L-type Ca^{2+} current.

Out of necessity, preparations of native adult CMs are dispersed and seeded as cultures of single cells. It is known that variance in cell density influences electrophysiological parameters[29], particularly within, and between, preparations of single cell preparations, including hiPSC-CMs[17]. Therefore, although the structural and function (eg, prevalent SR) maturity of adult native adult CMs from rabbit is an advantage over hiPSC-CMs, this is offset by the high level of heterogeneity of single cell preparations, which reduces the discrimination power. Although some of the differences will be due to the physiology of rabbit CMs relative to human CMs, we have also seen higher variability in human atrial trabeculae as compared with hiPSC-EHT; hence, there are separate challenges in using native cells. It is for these reasons we elected to use hiPSC-CMs within 2D or 3D syncytium, where individual cell-to-cell variability is averaged due to mechanical and electrical coupling. In addition, several studies have shown previously that the EHT format compared with standard 2D culture favors maturation in terms of MDP and upstroke velocity[30,31], structure[22], and metabolic preference[32].

Blinded analysis was done using serum-/protein-free medium, with the intention of avoiding protein-drug binding that might blunt the responses within the *in vitro* system. However, at least in the CO:R-PAT platform-cell combination, serum-/protein-free medium was a hindrance, leading to high spontaneous beat rates, and poor signal-to-noise ratio ratios. These issues were abrogated by using protein-containing medium (RPMI-B27), which enhanced the accuracy of predicting PIs on the CO:R-PAT platform from 0% to 75%. This indicates that, for this purpose, the benefits brought by the protein-containing medium outweigh the concerns of drug binding and batch-to-batch variations of protein ingredients. Nevertheless, voltage-sensitive dyes, such as FluoVolt, interact with proteins and reduce the signal-to-noise ratio, which make simultaneous recording of contraction and voltage challenging, although this may be

Table 1: Effects of compounds on cardiomyocyte contractility *in vitro*

Drugs were ranked by GSK personnel to provide a testing order, based on modes of action that were of interest to them. For each platform-cell combination, data listed represent mean maximum measurable percentage change relative to baseline for CA, CT, and RT. The concentration at which this effect occurred is listed but when it was different for CA, CT, and RT information is added after the relevant parameter. Green indicates the predicted effect matched the known effect on inotropy. Analysis platforms were CO (CellOPTIQEHT), EHT (engineered heart tissue) and TTM (Triple Transient Measurement). Cardiomyocyte types were rabbit adult cardiomyocytes (as comparator) or hiPSC lines: P-Cyte, (Pluricyte, Ncardia); iCell2 (Cellular Dynamics International); R-PAT (University of Nottingham); ERC18 (University of Hamburg).

Abbreviations: FPTC, free plasma therapeutic concentration; ACE, angiotensin converting enzyme; PDE, phosphodiesterase; SSR inhibitor, selective serotonin reuptake inhibitor; PI, positive inotrope; NI, negative inotrope; NE, no effect.

Compound	Rank	Mode of Action	Platform	Cell	CA	CT	RT	Test Range µM	Conc µM	FPTC µM	Known Effect	Blinded Assignment
Epinephrine	1	Nonselective α1-, β1-, and β2-adrenoceptor agonist	**CO**	**Rabbit**	+196	−26	+6 0.03 µM	0.01–1	0.1	0.0002–0.05	PI	**PI**
			TTM	**P-Cyte**	+53 0.03 µM	−34 1 µM	−9		0.01			**PI**
			CO	P-Cyte	+18 0.3 µM	+67 1 µM	−36		0.1			NE
			CO	**iCell2**	−12 0.3 µM	−43	+39		0.03			**PI**
			CO	R-PAT	+27 0.01 µM	+16	−18		1			NE
			EHT	**R-PAT**	+22	−16 1 µM	−22 0.3 µM		0.1			**PI**
			EHT	ERC18	+8	−6 1 µM	−7		0.01			NE

Compound	Rank	Mode of Action	Platform	Cell	CA	CT	RT	Test Range µM	Conc µM	FPTC µM	Known Effect	Blinded Assignment
Forskolin	2	Adenylyl cyclase stimulator	CO	Rabbit	−16	−34 0.1 µM	+45	0.1–10	3	0.012–0.024	PI	PI
			TTM	P-Cyte	+72 10 µM	−37 3 µM	−38		0.3			PI
			CO	P-Cyte	+31 1 µM	+55 3 µM	+47		0.3			NE
			CO	iCell2	−44	+64	+44		10			NI
			CO	R-PAT	−31 10 µM	−33	+20		0.1			NE
			EHT	R-PAT	+15 10 µM	−7	−22 3 µM		0.3			PI
			EHT	ERC18	+18 3 µM	−33	−23		10			PI
Levosimendan	3	Calcium sensitizer	CO	Rabbit	+16 0.1 µM	−33	−25	0.01–1	0.01	0.026–0.35	PI	NE
		PDE3 inhibitor	TTM	P-Cyte	+42 0.1 µM	+11 0.3 µM	−12		0.03			NE
		KATP channel agonist	CO	P-Cyte	−54	+54	−40		0.03			NE
			CO	iCell2	+14 0.3 µM	+80	+54		0.1			NE
			CO	R-PAT	+23 0.1 µM	−12	22 1 µM		0.01			NE
			EHT	R-PAT	+6	−7	−14 0.3 µM		0.01			NE
			EHT	ERC18	+13 1 µM	−9 0.1 µM	−4		0.01			NE
Pimobendan	4	Calcium sensitizer	CO	Rabbit	+132 1 µM	+72	+42	1–100	3	0.005–0.01	PI	NE
		PDE3 inhibitor	TTM	P-Cyte	+55	−31 10 µM	+73		30			NE
			CO	P-Cyte	−23 10 µM	+69	−19		3			NE
			CO	iCell2	+65	+69	−13 100 µM		1			NE
			CO	R-PAT	+18	+26 10 µM	+29		100			NE
			EHT	R-PAT	+12	−3.5	+12 100 µM		1			NE
			EHT	ERC18	+13 30 µM	−13	+14 100 µM		3			PI

Dobutamine	11	α1-, β1-, and β2-adrenoceptor agonist	CO	R-PAT	+39 3 μM	−16 10 μM	+29	0.1–10	0.3	0.07–1	PI	NE
			EHT	R-PAT	+44 3 μM	−25	−22		10			PI
			EHT	ERC18	+18 3 μM	−37 10 μM	+7		0.3			PI
Milrinone	13	PDE3 inhibitor	CO	R-PAT	−17	+16 3 μM	+15 100 μM	1–100	1	0.1–0.15	PI	NE
			EHT	R-PAT	+18	−11	−9		30			PI
			EHT	ERC18	+7	−18	−6 30 μM		100			PI
Omecamtiv mecarbil	14	Cardiac-specific myosin activator	CO	R-PAT	−47	+117	−34 0.01 μM	0.01–1	1	0.05–4.2	PI	NI
			EHT	R-PAT	+53	+37	−26		0.3			PI
			EHT	ERC18	+22	+38	−6 0.3 μM		1			PI
Terbutaline	21	β2-adrenoceptor agonist	CO	R-PAT	+28	−32 3 μM	−35 10 μM	0.1–10	0.3	1.3	PI	NE
			EHT	R-PAT	+17	−24	−35 0.3 μM		3			PI
			EHT	ERC18	+29 10 μM	−30	−17		1			PI
Verapamil	7	L-type calcium channel blocker, hERG blocker	CO	Rabbit	−82 0.03 μM	+24	+61	0.01–1	0.1	0.05	NI	NI
			TTM	P-Cyte	−79	−68	−11		0.1			NI
			CO	P-Cyte	(5/5)Q	(5/5)Q	(5/5)Q		1			NI
			CO	iCell2	(4/5)Q	+103 0.1 μM	(4/5)Q		1			NI
			CO	R-PAT	−98	−91	−88		1			NI
			EHT	R-PAT	(5/5)Q 0.1 μM	−7	−6		0.03			NI
			EHT	ERC18	(3/5)Q 0.3 μM	−25 0.1 μM	−17		0.1			NI

Compound	Rank	Mode of Action	Platform	Cell	CA	CT	RT	Test Range µM	Conc µM	FPTC µM	Known Effect	Blinded Assignment
Doxorubicin	8	Impairs Ca2+ transport mechanisms in SR	TTM	P-Cyte	−47	−46	+51	0.1–10	100	1–2	NI	NE
			CO	P-Cyte	−15	+70	+72		100			NE
			CO	iCell2	+65	−39	+57 30 µM		1			NE
			CO	R-PAT	−27 100 µM	+41 30 µM	−12		1			NE
Sunitinib	9	Multitargeted TK inhibitor	CO	Rabbit	−78	+46	+300	0.1–10	10	0.003	NI	NI
			TTM	P-Cyte	+42	−23 10 µM	+28		0.1			NI
			CO	P-Cyte	(5/5)Q	+163 0.1 µM	(5/5)Q		10			NI
			CO	iCell2	−25 10 µM	−43	+62		1			NI
			CO	R-PAT	−20	+34 0.1 µM	+33		10			NE
			EHT	R-PAT	+11	+6	+4 0.1 µM		0.3			NE
			EHT	ERC18	−8	+6	−8		3			NE
Citalopram	16	SSR inhibitor, hERG & L-type calcium channel blocker	CO	R-PAT	(10/10)Q	(10/10)Q	(10/10)Q	1–100	30	0.05	NI	NI
			EHT	R-PAT	(4/4)Q 10 µM	−6 3 µM	+5		1			NI
			EHT	ERC18	(5/5)Q 10 µM	+2 1 µM	+7		3			NI
Itraconazole	18	Triazole antifungal, mechanism unclear	CO	R-PAT	(5/5)Q	(5/5)Q	(5/5)Q	0.1–10	10	0.00086	NI	NI
			EHT	R-PAT	−51	+14 0.1 µM	−33		3			NI
			EHT	ERC18	(5/5)Q 10 µM	+11	−29 3 µM		1			NI

Sorafenib	19	Multitargeted TK inhibitor	CO	R-PAT	(10/10)Q	(10/10)Q	(10/10)Q	0.1–10	10	0.03	NI	NI
			EHT	R-PAT	−50	+14	+6 3 μM		10			NI
			EHT	ERC18	−56	+6 3 μM	−24		10			NI
Ivabradine	20	If inhibitor	CO	R-PAT	+46	+22	+24 0.3 μM	0.1–10	0.1	0.01–0.1	NI	NE
			EHT	R-PAT	−16	−27	+3 0.1 μM		10			NI
			EHT	ERC18	−56	14	+45		10			NI
Flecainide	22	Sodium channel blocker, hERG blocker	CO	R-PAT	+31	+26 10 μM	+29 1 μM	0.1–10	0.1	0.2–0.4	NI	NE
			EHT	R-PAT	(6/6)Q 3 μM	−16	−26 1 μM		0.3			NI
			EHT	ERC18	−74 10 μM	−21	+42		3			NI
Phentolamine	24	Nonselective α-adrenoceptor antagonist	CO	R-PAT	(5/5)Q	(5/5)Q	(5/5)Q	1–100	30	2.25	NI	NI
			EHT	R-PAT	5/5)Q 10 μM	−18	−28		3			NI
			EHT	ERC18	(5/5)Q	−30	+53		10			NI
Zimelidine	28	SSR inhibitor	EHT	R-PAT	18 1 μM	−15	−22	1–100	3	0.78	NI	NI
			EHT	ERC18	(5/5)Q 100 μM	−25 30 μM	+43		3			NI
Acetylsalicylic acid	5	Cyclooxygenase inhibitor	CO	Rabbit	+26	−21	−13	10–1000	100	0.3–2	NE	NE
			TTM	P-Cyte	+34	−8 1000 μM	+24 100 μM		10			NE
			CO	P-Cyte	−21 30 μM	−35	+20		10			NE
			CO	iCell2	−58 30 μM	−44	+47 1000 μM		10			NE
			CO	R-PAT	+23	−26 300 μM	+17 1000 μM		100			NE
			EHT	R-PAT	−14	+8 100 μM	+15		1000			NE
			EHT	ERC18	+8 300 μM	−8	−15		1000			NE

Compound	Rank	Mode of Action	Platform	Cell	CA	CT	RT	Test Range µM	Conc µM	FPTC µM	Known Effect	Blinded Assignment
Atenolol	6	β1 > β2 adrenoceptor antagonist	CO	Rabbit	+16	−13	+968 0.3 µM	0.1–10	1	1	NE	NE
			TTM	P-Cyte	+54	+8	−19 3 µM		1			NE
			CO	P-Cyte	−29	−71 10 µM	+69 3 µM		1			NE
			CO	iCell2	−42 0.1 µM	+58	−52		0.3			NE
			CO	R-PAT	−28 3 µM	+11	+11 10 µM		0.3			NE
			EHT	R-PAT	−25	+7 1 µM	+14		10			NE
			EHT	ERC18	+3	−13	−9 3 µM		10			NE
Captopril	10	ACE inhibitor	CO	Rabbit	−91	+72	+212	1–100	100	1–2	NE	NI
			TTM	P-Cyte	+136	−5	−14 10 µM		1			NE
			CO	P-Cyte	+24 30 µM	+132	−38		100			NE
			CO	iCell2	−27	+15 3 µM	−20 10 µM		1			NE
			CO	R-PAT	+18 3 µM	−26	−16 30 µM		1			NE
			EHT	R-PAT	−18	−7 100 µM	−9 10 µM		3			NE
			EHT	ERC18	+7	−10	−6 1 µM		3			NE
Glibenclamide	12	KATP channel antagonist	CO	Rabbit	+66 1 µM	−27 0.3 µM	+61	0.1–10	0.1	0.02–0.06	NE	NE
			CO	R-PAT	+36	−26 10 µM	+31		0.1			NE
			EHT	R-PAT	+3	+6	−12		1			NE
			EHT	ERC18	+6	+10	−5 3 µM		10			NE
Enalaprilat	15	ACE inhibitor	CO	R-PAT	+54	+20 10 µM	+34	1–100	100	0.12	NE	NE
			EHT	R-PAT	+33	+5 1 µM	−14		30			PI
			EHT	ERC18	+2 10 µM	−3	−4		100			NE

Clonidine	17	α2-adrenoceptor agonist	CO	R-PAT	−24	+26	−27	0.01–1	0.3	0.002–0.004	NE	NE
			EHT	R-PAT	+10	+11 0.1 μM	−12		0.3			NE
			EHT	ERC18	+5 0.3 μM	+5	+4		0.1			NE
Paracetamol	23	Prostaglandin synthesis inhibitor	CO	R-PAT	+19 100 μM	+26	+13 1000 μM	10–1000	30	50	NE	NE
			EHT	R-PAT	−19	−20	−9 100 μM		1000			NE
			EHT	ERC18	+3 100 μM	−9	+10		1000			NE
Tolbutamide	25	KATP channel antagonist, adenylyl cyclase stimulator	CO	R-PAT	+35	−16 10 μM	+45	1–100	100	20–30	NE	NE
			EHT	R-PAT	−12	+9	−8 10 μM		1			NE
			EHT	ERC18	+21	−3	−9		100			PI
Pravastatin	26	HMG CoA reductase inhibitor	CO	R-PAT	+53	+42	+12 1 μM	1–100	3	0.018	NE	NE
			EHT	R-PAT	−19	−15 30 μM	13 100 μM		3			NE
			EHT	ERC18	+19	+3 30 μM	−11 100 μM		10			PI
Sildenafil	27	PDE5 inhibitor	CO	R-PAT	+56	+39	+30 3 μM	0.3 – 30	10	0.02	NE	NE
			EHT	R-PAT	−10	−16	+13 3 μM		10			NE
			EHT	ERC18	+9	−4 10 μM	−6		1			NE

Table 2: Predictivity tables and scores

Collective data are presented for cross comparison between platform-cell combinations relating to the 9 drugs tested in common or all drugs evaluated. Green shading shows predictivity of > 75%, orange of 50%–74%, and red of < 50%. Predictivity is gauged as whether the assignment made by the investigators matched the assignment made by the commercial sponsor, GlaxoSmithKline, and the available literature described in Supplementary Table 1.

Platform:Cell Combination		Config.	Nine Drugs in Common				All Drugs Assessed			
			PI (%)	NI (%)	NE (%)	Total (%)	PI (%)	NI (%)	NE (%)	Total (%)
CellOPTIQ	Rabbit CMs	2D	2/4 (50)	2/2 (100)	2/3 (67)	6/9 (67)	2/4 (50)	2/2 (100)	3/4 (75)	7/10 (70)
TTM	Pluricyte hiPSC-CMs		2/4 (50)	2/2 (100)	3/3 (100)	7/9 (78)	2/4 (50)	2/3 (67)	3/3 (100)	7/10 (70)
CellOPTIQ	Pluricyte hiPSC-CMs		0/4 (0)	2/2 (100)	3/3 (100)	5/9 (56)	0/4 (0)	2/3 (67)	3/3 (100)	5/10 (50)
	iCell2 hiPSC-CMs		1/4 (25)	2/2 (100)	3/3 (100)	6/9 (67)	1/4 (25)	2/3 (67)	3/3 (100)	6/10 (60)
	R-PAT hiPSC-CMs		0/4 (0)	1/2 (50)	3/3 (100)	4/9 (44)	0/8 (0)	5/9 (56)	10/10 (100)	15/27 (56)
EHT	R-PAT hiPSC-CMs	3D	2/4 (50)	1/2 (50)	3/3 (100)	6/9 (67)	6/8 (75)	8/9 (89)	9/10 (90)	23/27 (85)
	ERC hiPSC-CMs		2/4 (50)	1/2 (50)	3/3 (100)	6/9 (67)	6/8 (75)	8/9 (89)	8/10 (80)	22/27 (81)

overcome by measuring extracellular voltage.

Treatment of hiPSC-CMs with doxorubicin for 30 min caused changes in electrophysiology (eg, triangulation, see web tool) and hence gave a distinctive response compared with NEs such as acetylsalicylic acid. Nevertheless, this acute exposure did not always cause changes in inotropy, which shows the importance of examining an appropriate concentration range and/or exposure times of drugs. Increasing exposure time to approximately 1–7 days unveiled doxorubicin and sunitinib as NIs, consistent with the extended timescale over which cardiac toxicity presents clinically and is in line with data from a previous study using TKI-inhibitor[33]. Interestingly, with 24 h of doxorubicin treatment, the CO:R-PAT platform-cell combination appeared to show a trend of positive inotropy from 1 to 30 μM (increased CA; decreased CT) but cell death at 10 μM. This aligns with reports indicating the effects of doxorubicin are complex in that transient positive inotropy is followed by robust negative inotropy at higher concentrations[34-36].

The levels of accuracy of up to 93% in predicting drug-induced changes in contractility in human hearts under these refined conditions are favorable relative to those from animal model[37,38]. They are also comparable with data using 3D cardiac microtissues containing hiPSC-CMs, cardiac endothelial cells, and cardiac fibroblasts, which correctly predicted 23 of 29 (85%) inotropes across a nonblinded panel of compounds[15]. These findings are encouraging, but it is not always straightforward to translate hiPSC-CM-related parameters of CA, CT, RT, and chronotropy (beat rate) to clinically relevant data. We have suggested that data derived from hiPSC-CMs on CA is informative for NIs in all cell-platforms combinations and for PIs in the 3D EHT platform. However, in the 2D systems, CT, and RT may be informative for PIs. We have considered different explanations for this observation. If 2D systems are less adept at showing an increase in CA, then decreases in CT (clinotropy; also expressed as an increase in dF/dt) or decreases in RT (lusitropy; also expressed as an increase in −dF/dt) become more important. By considering pF/dt values, which can change independently of the peak force, there is alignment with the effects seen *in vivo*, which are often expressed as a change in dP/dt_{max} or $-dP/dt_{min}$. An alternative explanation is that, although this is not automatically intuitive, it may be a quirk of hiPSC-CMs; as a model system, there are limitations and adaptations in thinking need to be made. Nevertheless, the robustness of this notion will need to be tested on a wider range of drugs to determine whether these *in vitro* parameters are relevant to *in vivo* cardiac physiology.

Effects on cardiac contractility per se may not indicate or predict a clinically relevant detrimental effect on the heart. For example, cardio-active L-type calcium channel blockers are used for treatment of hypertension. Additional "structural" endpoints, such as mitochondrial membrane permeability (Δψm), endoplasmic reticulum integrity, contractile filament expression/organization, ATP depletion, and cardiac troponin levels in hiPSC-CM-based assay platforms may add interpretive value to functional changes[20]. A limitation of our study was that some modes of action were not represented in the drug panel, such as the SERCA activator CDN1163[39,40], or the myosin inhibitor blebbistatin[41], and these would be interesting to include in blinded assays in the future.

In our study, we looked for trends or significant changes in the parameters measured, but did not apply a cut off on how much change was considered meaningful (e.g. > 15% change and statistical significance). Whether analysis can be modified in the future is for consideration but would need to be done with care. The NE drugs, enalaprilat, tolbutamide, and pravastatin caused changes of 19%–33% in CA on the EHT platform and were incorrectly predicted as PIs. However, these magnitudes of changes were similar or greater than those recorded for PIs, and so adding thresholds on CA would not have improved prediction and could have been detrimental. Relationship to FTPC was not a strong association either, with the maximum changes of the incorrectly predicted NEs varying from 3-fold below the FTPC (tolbutamide) to > 100-fold above (enalaprilat, pravastatin). This also underscores the importance of technical precision and inclusion of time controls in each single experiment, particularly in strategies employing cumulative concentration-response analyses which take time.

These observations likely reflect the complexity of drug-cell interactions, which means differential effects can occur dependent on the concentration and categorizing as PI, NI, and NE was difficult in some cases. Inotropic effects of high concentrations of sulphonylureas, such as tolbutamide, have been reported for *in vitro* systems[42]. Angiotensin converting enzyme (ACE) inhibitors, such as enalaprilat, lead to bradykinin accumulation and thereby lead to bradykinin B1 receptor activation, which elevates intracellular Ca^{2+} and causes a positive inotropic effect[43]. Similarly, phentolamine is a neutral inotrope at free plasma concentrations of approximately 2.5 µM in patients[44], but at concentrations above 10 µM phentolamine causes negative inotropy via modulation of fast sodium and L-type calcium channels[45,46]. This is consistent with our data, indicating that there are multiple pharmacological effects of this compound. For ivabradine the concentrations provided were much higher than the FTPC, which can lead to off-target effects of poorly selective drugs[47]. In some cases, such as zimelidine, the difficulty arose due to lack of robust *in vitro* data within the literature[48-50]. Care must therefore be used when (1) selecting test compounds by primary pharmacology and (2) using *in vitro* assay paradigms to predict *in vivo*, clinically relevant cardiotoxicity, either when used as a "screening assay" to rank compounds or as a reflex investigative assay, e.g. following detection of cardiotoxicity in animal toxicology studies.

Because PIs are cardio-active drugs, it might be expected that the FTPC aligns with responses from hiPSC-CMs. This was true for the EHT platform, where significant responses were within, or close to, the FTPC. However, both the pharmacologic or statistical sensitivity of 2D hiPSC-CM cultures and isolated single rabbit cardiomyocytes were considerably lower. Two explanations may account for these observations. First, the greater stability of CMs in 3D constructs permitted cumulative dosing of EHTs within the same well, which created tighter datasets than the 2D systems, where parallel dosing in separate well was required. Second, in contrast to 2D monolayers that evaluated hiPSC-CM movement in unloaded conditions, the EHT platform measures force of contraction under loaded conditions[52]. This facilitates maturation and Frank-Starling mechanisms for force generation are followed, leading to higher basal tone and cAMP signaling[42,52]), which are important modes of action of the PIs epinephrine, forskolin, and milrinone. Consistent with this, positive inotropy of milrinone was shown in "Biowire II" tissue engineered constructs, which also places hiPSC-CMs under loaded

conditions to facilitate maturation[53].

To measure whole heart function and its integration with neurohormonal or hemodynamic feedback, numerous assessment parameters are used, including P_{max}, dP/dt_{max} (max rate of change if pressure) and left ventricular ejection fraction[54]. Atenolol, a selective β1-adrenoceptor antagonist, requires intact sympathetic innervation and is an NI in the clinic but shows NE in hiPSC-CMs[55,56]. Similarly, the mode of action for clonidine is through presynaptic alpha-adrenoceptors on sympathetic neurons with the consequence of reduced sympathetic drive and its effect on heart function (reduced heart rate and force)[57,58], but these effects would not be detected in a "cardiomyocyte only" model. Predictive screening will also benefit from inclusion of auxiliary cell types, such as neural lineages to enable evaluation of drugs that work via the neurohormonal system.

Other issues that need to be considered for the future include throughput, user variability, cell availability, cost, and batch-to-batch variability. Although the TTM platform allowed simultaneous measurement of contraction, Ca^{2+} handling, and voltage, the low throughput meant that only 10 drugs were evaluated in 1 hiPSC-CM line. User variability has been noted in other studies. For example, variations in TdP predictability across different sites using identical instruments were reported in the CiPA study, and so could be a factor in the site to site differences we observed. Cost was another factor, wherein each drug assessed typically required 1.6 million (40 wells in a 96-well plate) and 5 million (5 EHTs) hiPSC-CMs, corresponding to up to approximately $3000 per drug at current prices. For these reasons, most of the assays in this report were done using hiPSC-CMs produced "in house," where cost for 1.6 or 5 million cells is approximately $16 or $50, respectively, albeit without the same level of quality control of commercial cells. Nevertheless, for both in house and commercial cells, batch-to-batch variation meant that the drug assays need to be repeated. These issues become more prominent when larger tissue engineered constructs are used. For example, "heart-in-a-jar" technologies, produce miniature 3D engineered electro-mechanically coupled cardiac organoid chamber that mimic pumping action similar to natural heart but require 10 million hiPSC-CM[59]. Thus, it is encouraging that scaled production of hiPSC-CMs is now becoming relatively routine and so costs should decrease in the near future.

Altogether, this study suggests that, even in their current status of technology evolution, hiPSC-CMs cultured in 2D and 3D may have value to predictive safety pharmacology. Given the high resource and costs involved with drug development, even modest improvements in the pipeline could have large socioeconomic and 3R benefits. More than 6000 putative medicines are in preclinical development, using millions of animals at an annual total cost of $11.3Bn, and so each percentile reduction equates to approximately $100 M. Similarly, reducing drug attrition in phase 1 clinical trials by 5% could reduce development costs by 5.5%–7.1%. Building on our work with further improvement and validation studies, conducted in a blinded manner, will facilitate uptake of hiPSC-CMs as a routine tool in safety pharmacology.

Funding

National Centre for the Replacement, Refinement & Reduction of Animals in Research (CRACK-IT: 35911-259146, NC/K000225/1); the British Heart Foundation (SP/15/9/31605, RG/15/6/31436, PG/14/59/31000, RG/14/1/30588, P47352/CRM); the German Research Foundation (DFG-Es-88/12-1, HA3423/5-1); European Research Council (ERC-AG-IndivuHeart, ERC-AdG STEMCARDIOVASC); Netherlands Science Foundation (NWO) under the Gravitation Grant "NOCI" Program (024.003.001); European Commission (FP7-Biodesign); German Centre for Cardiovascular Research (DZHK) and the German Ministry of Education and Research, the Freie und Hansestadt Hamburg; ZonMW (ZorgOnderzoek Nederland—Medische wetenschappen); MKMD (Meer Kennis met Minder Dieren) Applications of Innovations 2015–2016.

References

1. Catapult. (2018). State of the discovery nation 2018 and the role of the medicines discovery catapult. Available at: https://s3-eu-west-1.amazonaws.com/media.newmd.catapult/wp-content/uploads/2018/01/16220811/MDC10529-Thought-Leader_v10_Interactive_v1.pdf.

2. IFPMA. (2017). International Federation of Pharmaceutical Manufacturers and Associations. The Pharmaceutical Industry and Global Health Facts and Figure. Geneva, Switzerland. Available at: https://www.ifpma.org/wp-content/uploads/2017/02/IFPMA-Facts-And-Figures-2017.pdf.

3. Onakpoya I. J., Heneghan C. J., Aronson J. K. Post-marketing withdrawal of 462 medicinal products because of adverse drug reactions: A systematic review of the world literature. *BMC Med.* **14,** 10 (2016).

4. Fuentes A. V., Pineda M. D., Venkata K. Comprehension of top 200 prescribed drugs in the US as a resource for pharmacy teaching, training and practice. *Pharmacy* **6,** 43 (2018).

5. Shah R. R. Can pharmacogenetics help rescue drugs withdrawn from the market? *Pharmacogenomics* **7,** 889–908 (2006).

6. Food Drug Administration HHS. International Conference on Harmonisation; guidance on S7B nonclinical evaluation of the potential for delayed ventricular repolarization (QT interval prolongation) by human pharmaceuticals; availability. *Notice. Fed. Regist*. **70,** 61133–61134 (2005).

7. Food Drug Administration HHS. International Conference on Harmonisation; guidance on E14 clinical evaluation of QT/QTc interval prolongation and proarrhythmic potential for non-antiarrhythmic drugs; availability. *Notice. Fed. Regist.* **70,** 61134–61135 (2005).

8. Gintant G. An evaluation of hERG current assay performance: Translating preclinical safety studies to clinical QT prolongation. *Pharmacol. Ther.* **129,** 109–119 (2011).

9. Gintant G., Fermini B., Stockbridge N., Strauss D. The evolving roles of human iPSC-derived cardiomyocytes in drug safety and discovery. *Cell Stem Cell* **21,** 14–17 (2017).

10. Fermini B., Hancox J. C., Abi-Gerges N., Bridgland-Taylor M., Chaudhary K. W., Colatsky T., Correll K., Crumb W., Damiano B., Erdemli G., et al. A new perspective in the field of cardiac safety testing through the Comprehensive *in vitro* Proarrhythmia Assay paradigm. *J. Biomol. Screen*. **21,** 1–11 (2016).

11. Kanda Y., Yamazaki D., Osada T., Yoshinaga T., Sawada K. Development of torsadogenic risk assessment using human induced pluripotent stem cell-derived cardiomyocytes: Japan iPS cardiac safety assessment (JiCSA) update. *J. Pharmacol. Sci.* **138,** 233–239 (2018).

12. Sager P. T., Gintant G., Turner J. R., Pettit S., Stockbridge N. Rechanneling the cardiac proarrhythmia safety paradigm: A meeting report from the cardiac safety research consortium. *Am. Heart J.* **167,** 292–300 (2014).

13. Blinova K., Dang Q., Millard D., Smith G., Pierson J., Guo L., Brock M., Lu H. R., Kraushaar U., Zeng H., et al. International multisite study of human-induced pluripotent stem cell-derived cardiomyocytes for drug proarrhythmic potential assessment. *Cell Rep.* **24,** 3582–

3592 (2018).

14. Bot C. T., Juhasz K., Haeusermann F., Polonchuk L., Traebert M., Stoelzle-Feix S. Cross—Site comparison of excitation-contraction coupling using impedance and field potential recordings in hiPSC cardiomyocytes. *J. Pharmacol. Toxicol. Methods* **93,** 46–58 (2018).

15. Pointon A., Pilling J., Dorval T., Wang Y., Archer C., Pollard C. High-throughput imaging of cardiac microtissues for the assessment of cardiac contraction during drug. *Toxicol. Sci.* **155,** 444–457 (2017).

16. van Meer B. J., Krotenberg A., Sala L., Davis R. P., Eschenhagen T., Denning C., Tertoolen L. G. J., Mummery C. L. Simultaneous measurement of excitation-contraction coupling parameters identifies mechanisms underlying contractile responses of hiPSC-derived cardiomyocytes. *Nat. Commun.* **10,** 4325 (2019).

17. Mosqueira D., Mannhardt I., Bhagwan J. R., Lis-Slimak K., Katili P., Scott E., Hassan M., Prondzynski M., Harmer S. C., Tinker A., et al. CRISPR/Cas9 editing in human pluripotent stem cell-cardiomyocytes highlights arrhythmias, hypocontractility, and energy depletion as potential therapeutic targets for hypertrophic cardiomyopathy. *Eur. Heart J.* **39,** 3879–3892 (2018).

18. Smith J. G. W., Owen T., Bhagwan J. R., Mosqueira D., Scott E., Mannhardt I., Patel A., Barriales-Villa R., Monserrat L., Hansen A., et al. Isogenic pairs of hiPSC-CMs with hypertrophic cardiomyopathy/LVNC-associated ACTC1 E99K mutation unveil differential functional deficits. *Stem Cell Rep.* **11,** 1226–1243 (2018).

19. Breckwoldt K., Letuffe-Breniere D., Mannhardt I., Schulze T., Ulmer B., Werner T., Benzin A., Klampe B., Reinsch M. C., Laufer S., et al. Differentiation of cardiomyocytes and generation of human engineered heart tissue. *Nat. Protoc.* **12,** 1177–1197 (2017).

20. Sala L., van Meer B. J., Tertoolen L. G. J., Bakkers J., Bellin M., Davis R. P., Denning C., Dieben M. A. E., Eschenhagen T., Giacomelli E., et al. MUSCLEMOTION: A versatile open software tool to quantify cardiomyocyte and cardiac muscle contraction *in vitro* and *in vivo*. *Circ. Res.* **122,** e5–16 (2018).

21. Duncan G., Firth K., George V., Hoang M. D., Staniforth A., Smith G., Denning C. Drug-mediated shortening of action potentials in LQTS2 human induced pluripotent stem cell-derived cardiomyocytes. *Stem Cells Dev.* **26,** 1695–1705 (2017).

22. Mannhardt I., Breckwoldt K., Letuffe-Breniere D., Schaaf S., Schulz H., Neuber C., Benzin A., Werner T., Eder A., Schulze T., et al. Human engineered heart tissue: Analysis of contractile force. *Stem Cell Rep.* **7,** 29–42 (2016).

23. Butler L., Cros C., Oldman K. L., Harmer A. R., Pointon A., Pollard C. E., Abi-Gerges N. Enhanced characterization of contractility in cardiomyocytes during early drug safety assessment. *Toxicol. Sci.* **145,** 396–406 (2015).

24. Bois P., Bescond J., Renaudon B., Lenfant J. Mode of action of bradycardic agent, S 16257, on ionic currents of rabbit sinoatrial node cells. *Br. J. Pharmacol.* **118,** 1051–1057 (1996).

25. Malik F. I., Hartman J. J., Elias K. A., Morgan B. P., Rodriguez H., Brejc K., Anderson R. L., Sueoka S. H., Lee K. H., Finer J. T., et al. Cardiac myosin activation: A potential therapeutic approach for systolic heart failure. *Science* **331,** 1439–1443 (2011).

26. Allen D. G., Eisner D. A., Pirolo J. S.,

Smith G. L. The relationship between intracellular calcium and contraction in calcium-overloaded ferret papillary-muscles. *J. Physiol. Lond.* **364,** 169–182 (1985).

27. Hess P., Wier W. G. Excitation-contraction coupling in cardiac Purkinje-fibers—Effects of caffeine on the intracellular Ca-2+ transient, membrane currents, and contraction. *J. Gen. Physiol.* **83,** 417–433 (1984).

28. Knollmann B. C. Induced pluripotent stem cell-derived cardiomyocytes boutique science or valuable arrhythmia model? *Circ. Res.* **112,** 969–976 (2013).

29. Du D. T. M., Hellen N., Kane C., Terracciano C. Action potential morphology of human induced pluripotent stem cell-derived cardiomyocytes does not predict cardiac chamber specificity and is dependent on cell density. *Biophys. J.* **108,** 1–4 (2015).

30. Lemoine M. D., Mannhardt I., Breckwoldt K., Prondzynski M., Flenner F., Ulmer B., Hirt M. N., Neuber C., Horváth A., Kloth B., et al. Human iPSC-derived cardiomyocytes cultured in 3D engineered heart tissue show physiological upstroke velocity and sodium current density. *Sci. Rep.* **7,** 5464 (2017).

31. Lemoine M. D., Krause T., Koivumäki J. T., Prondzynski M., Schulze M. L., Girdauskas E., Willems S., Hansen A., Eschenhagen T., Christ T. Human induced pluripotent stem cell-derived engineered heart tissue as a sensitive test system for QT prolongation and arrhythmic triggers. *Circ. Arrhythm. Electrophysiol.* **11,** e006035 (2018).

32. Ulmer B. M., Stoehr A., Schulze M. L., Patel S., Gucek M., Mannhardt I., Funcke S., Murphy E., Eschenhagen T., Hansen A. Contractile work contributes to maturation of energy metabolism in hiPSC-derived cardiomyocytes. *Stem Cell Rep.* **10,** 834–847 (2018).

33. Jacob F., Yonis A. Y., Cuello F., Luther P., Schulze T., Eder A., Streichert T., Mannhardt I., Hirt M. N., Schaaf S., et al. Analysis of tyrosine kinase inhibitor-mediated decline in contractile force in rat engineered heart tissue. *PLoS One* **11,** e0145937 (2016).

34. Kim D. H., Akera T., Brody T. M. Inotropic actions of doxorubicin in isolated guinea-pig atria—Evidence for lack of involvement of Na+, K+-adenosine triphosphatase. *J. Pharmacol. Exp. Ther.* **214,** 368–374 (1980).

35. Vanboxtel C. J., Olson R. D., Boerth R. C., Oates J. A. Doxorubicin—Inotropic effects and inhibitory action on ouabain. *J. Pharmacol. Exp. Ther.* **207,** 277–283 (1978).

36. Wang Y. X., Korth M. Effects of doxorubicin on excitation-contraction coupling in guinea-pig ventricular myocardium. Circ. Res. 76, 645–653 (1995).

37. Lawrence C. L., Pollard C. E., Hammond T. G., Valentin J. P. *In vitro* models of proarrhythmia. *Br. J. Pharmacol.* **154,** 1516–1522 (2008).

38. Valentin J.-P., Bialecki R., Ewart L., Hammond T., Leishmann D., Lindgren S., Martinez V., Pollard C., Redfern W., Wallis R. A framework to assess the translation of safety pharmacology data to humans. *J. Pharmacol. Toxicol. Methods* **60,** 152–158 (2009).

39. Dahl R. A new target for Parkinson's disease: Small molecule SERCA activator CDN1163 ameliorates dyskinesia in 6-OHDA-lesioned rats. *Bioorg. Med. Chem.* **25,** 53–57 (2017).

40. Kang S., Dahl R., Hsieh W., Shin A.,

Zsebo K. M., Buettner C., Hajjar R. J., Lebeche D. Small molecular allosteric activator of the sarco/endoplasmic reticulum Ca^{2+}-ATPase (SERCA) attenuates diabetes and metabolic disorders. *J. Biol. Chem.* **291,** 5185–5198 (2016).

41. Kovacs M., Toth J., Hetenyi C., Malnasi-Csizmadia A., Sellers J. R. Mechanism of blebbistatin inhibition of myosin II. *J. Biol. Chem.* **279,** 35557–35563 (2004).

42. Huupponen R. Adverse cardiovascular effects of sulfonylurea drugs clinical-significance. Med. Toxicol. 2, 190–209 (1987).

43. Ignjatovic T., Tan F. L., Brovkovych V., Skidgel R. A., Erdos E. G. Activation of bradykinin B-1 receptor by ACE inhibitors. *Int. Immunopharmacol.* **2,** 1787–1793 (2002).

44. Wallis R., Gharanei M., Maddock H. Predictivity of *in vitro* non-clinical cardiac contractility assays for inotropic effects in humans—A literature search. *J. Pharmacol. Toxicol. Methods* **75,** 62–69 (2015).

45. Rosen M. R., Gelband H., Hoffman B. F. Effects of phentolamine on electrophysiologic properties of isolated canine purkinje fibers. *J. Pharmacol. Exp. Ther.* **179,** 586–593 (1971).

46. Sada H. Effect of phentolamine, alprenolol and prenylamine on maximum rate of rise of action potential in guinea-pig papillary-muscles. *Naunyn Schmiedebergs Arch. Pharmacol.* **304,** 191–201 (1978).

47. Choi H. Y., Bae K.-S., Cho S.-H., Ghim J.-L., Choe S., Jung J. A., Lim H.-S. Population plasma and urine pharmacokinetics of ivabradine and its active metabolite S18982 in healthy Korean volunteers. *J. Clin. Pharmacol.* **56,** 439–449 (2016).

48. Forsberg T., Lindbom L. O. . Cardiovascular effects of zimelidine and tricyclic anti-depressants in conscious rats. *Acta Pharmacol. Toxicol.* **53,** 223–229 (2009).

49. Lindbom L. O., Forsberg T. Cardiovascular effects of zimelidine and other antidepressant in conscious rats. *Acta Psychiatr. Scand. Suppl.* **63,** 380–384 (1981).

50. Naranjo C. A., Sellers E. M., Kaplan H. L., Hamilton C., Khouw V. Acute kinetic and dynamic interactions of zimelidine with ethanol. *Clin. Pharmacol. Ther.* **36,** 654–660 (1984).

51. Eder A., Vollert I., Hansen A., Eschenhagen T. Human engineered heart tissue as a model system for drug testing. *Adv. Drug Deliv. Rev.* **96,** 214–224 (2016).

52. Uzun A. U., Mannhardt I., Breckwoldt K., Horvath A., Johannsen S. S., Hansen A., Eschenhagen T., Christ T. Ca^{2+}-currents in human induced pluripotent stem cell-derived cardiomyocytes effects of two different culture conditions. *Front. Pharmacol.* **7,** 300 (2016).

53. Zhao Y., Rafatian N., Feric N. T., Cox B. J., Aschar-Sobbi R., Wang E. Y., Aggarwal P., Zhang B., Conant G., Ronaldson-Bouchard K., et al. A platform for generation of chamber-specific cardiac tissues and disease modeling. *Cell* **176,** 913–927.e18 (2019).

54. Guth B. D., Chiang A. Y., Doyle J., Engwall M. J., Guillon J.-M., Hoffmann P., Koerner J., Mittelstadt S., Ottinger S., Pierson J. B., et al. The evaluation of drug-induced changes in cardiac inotropy in dogs: Results from a HESI-sponsored consortium. *J. Pharmacol. Toxicol. Methods* **75,** 70–90 (2015).

55. Kaumann A. J., Blinks J. R. Stimulant and depressant effects of beta-adrenoceptor blocking-agents on isolated heart-muscle—A positive inotropic effect not mediated through adrenoceptors. *Naunyn Schmiedebergs Arch. Pharmacol.* **311,** 205–218 (1980).

56. Lemoine H., Schonell H., Kaumann A. J. Contribution of beta-1-adrenoceptors and beta-2-adrenoceptors of human atrium and ventricle to the effects of noradrenaline and adrenaline as assessed with (–)-atenolol. *Br. J. Pharmacol.* **95,** 55–66 (1988).

57. Jarrott B., Louis W. J., Summers R. J. Characteristics of clonidine-H-3 binding to an alpha-adrenoceptor in membranes from guinea-pig kidney. *Br. J. Pharmacol.* **65,** 663–670 (1979).

58. Kleiber N., Mathot R. A. A., Ahsman M. J., Wildschut E. D., Tibboel D., de Wildt S. N. Population pharmacokinetics of intravenous clonidine for sedation during paediatric extracorporeal membrane oxygenation and continuous venovenous hemofiltration. *Br. J. Clin. Pharmacol.* **83,** 1227–1239 (2017).

59. Li R. A., Keung W., Cashman T. J., Backeris P. C., Johnson B. V., Bardot E. S., Wong A. O. T., Chan P. K. W., Chan C. W. Y., Costa K. D. Bioengineering an electro-mechanically functional miniature ventricular heart chamber from human pluripotent stem cells. *Biomaterials* **163,** 116–127 (2018).

Supplementary information

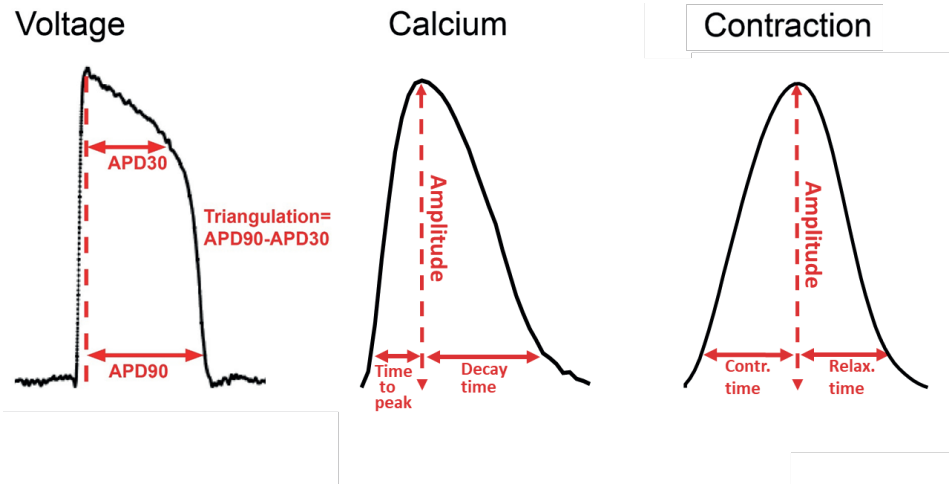

Supplementary Figure 1: Schematic description of the parameters used to quantify drug effect in hiPSC-CMs.

Data were calculated using the *MUSCLEMOTION* algorithm. APD, action potential duration.

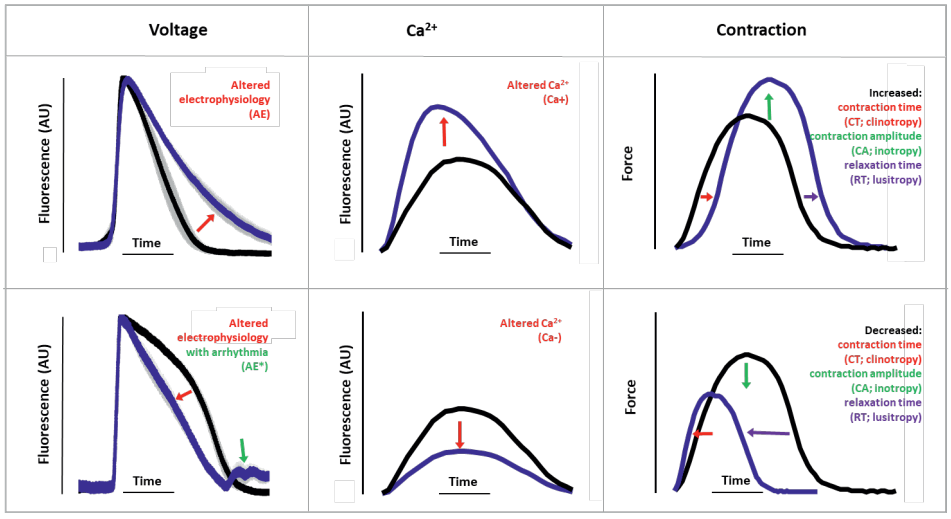

Supplementary Figure 2: Terminology used in evaluation of responses.

Black traces are baseline readings, while blue are after treatment. The colour of the arrows and text matches to indicate the type of change occurring.

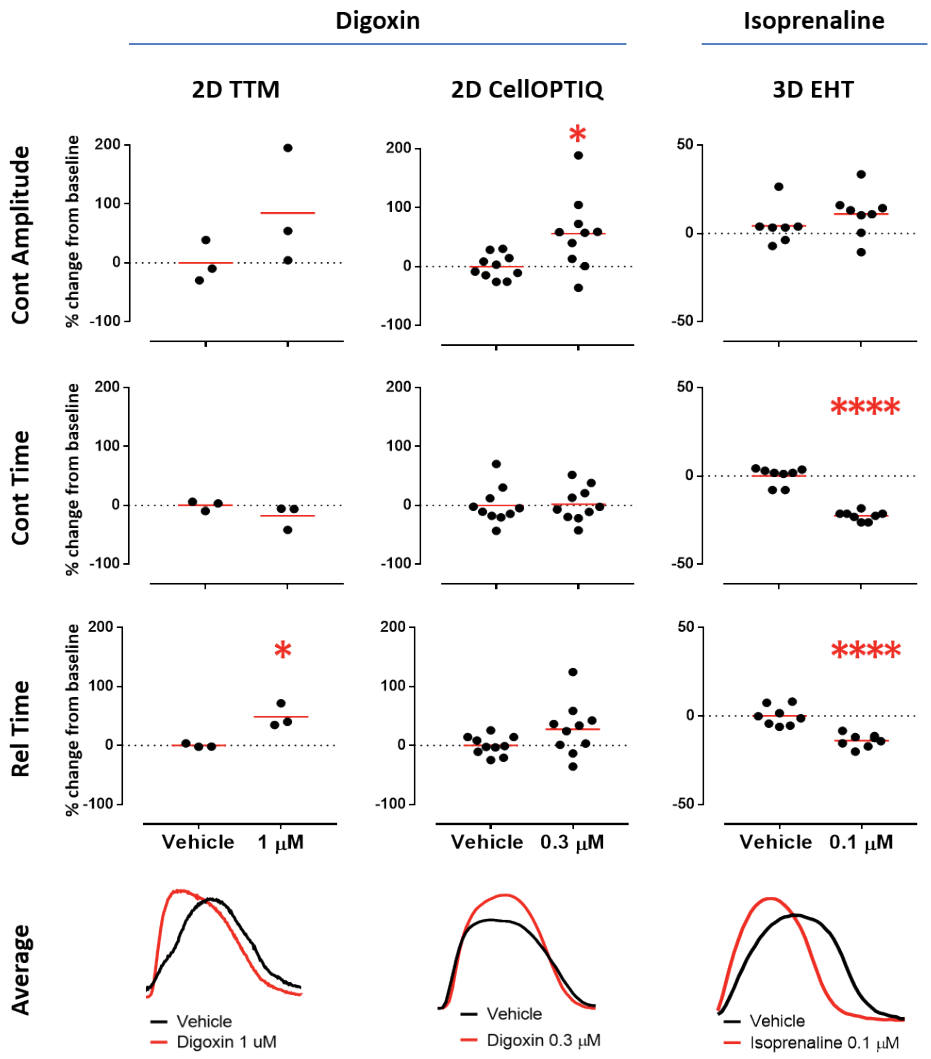

Supplementary Figure 3: Training sets to unify drug testing procedures.

Representative contractility data are shown for positive (digoxin, 2D; isoprenaline, 3D) and negative (nifedipine 2D, 3D) inotropes evaluated in hiPSC-CMs using the TTM (Triple Transient Measurement), CellOPTIQ® and EHT (engineered heart tissue) platforms. The percentage change in drug treated samples is relative to their respective vehicle control. Unpaired T-test. * p<0.05; ** p<0.01; *** p<0.001; **** p<0.0001.

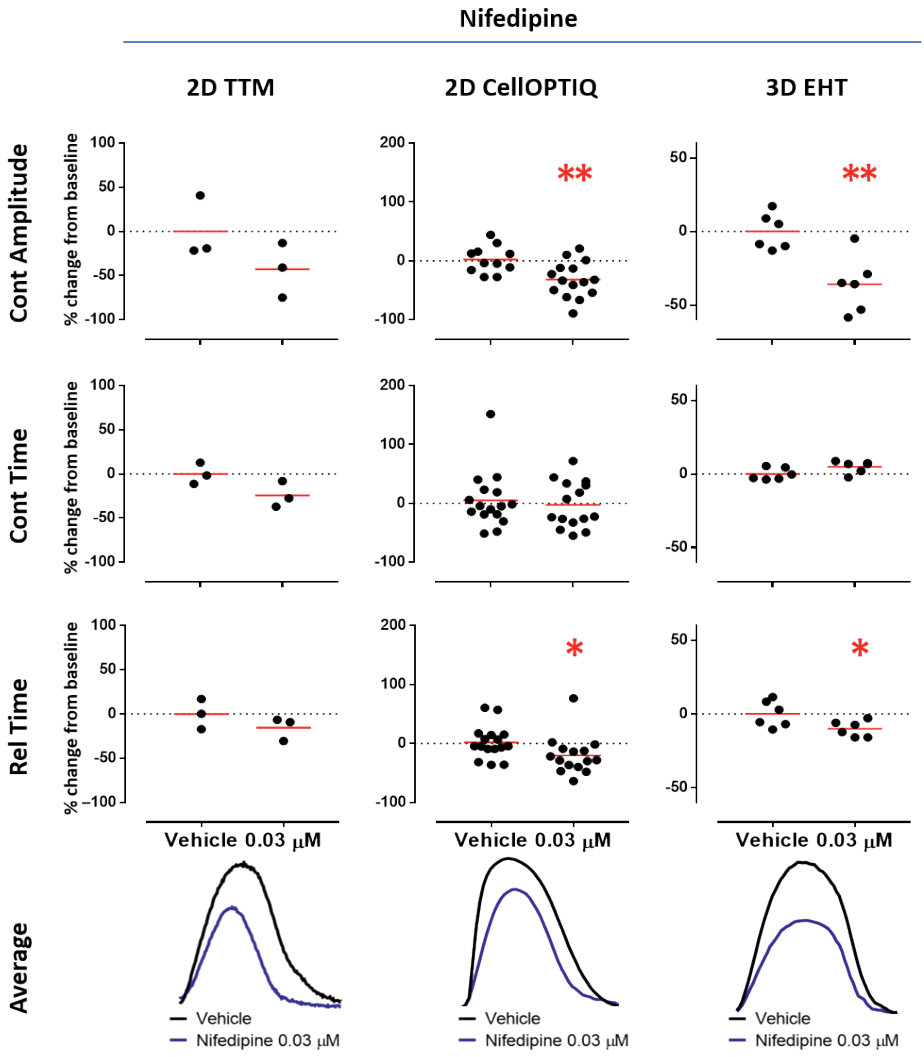
Nifedipine
2D TTM
2D CellOPTIQ
3D EHT
Cont Amplitude
Cont Time
Rel Time
Average
% change from baseline
**
*
Vehicle 0.03 μM
Vehicle
Nifedipine 0.03 μM

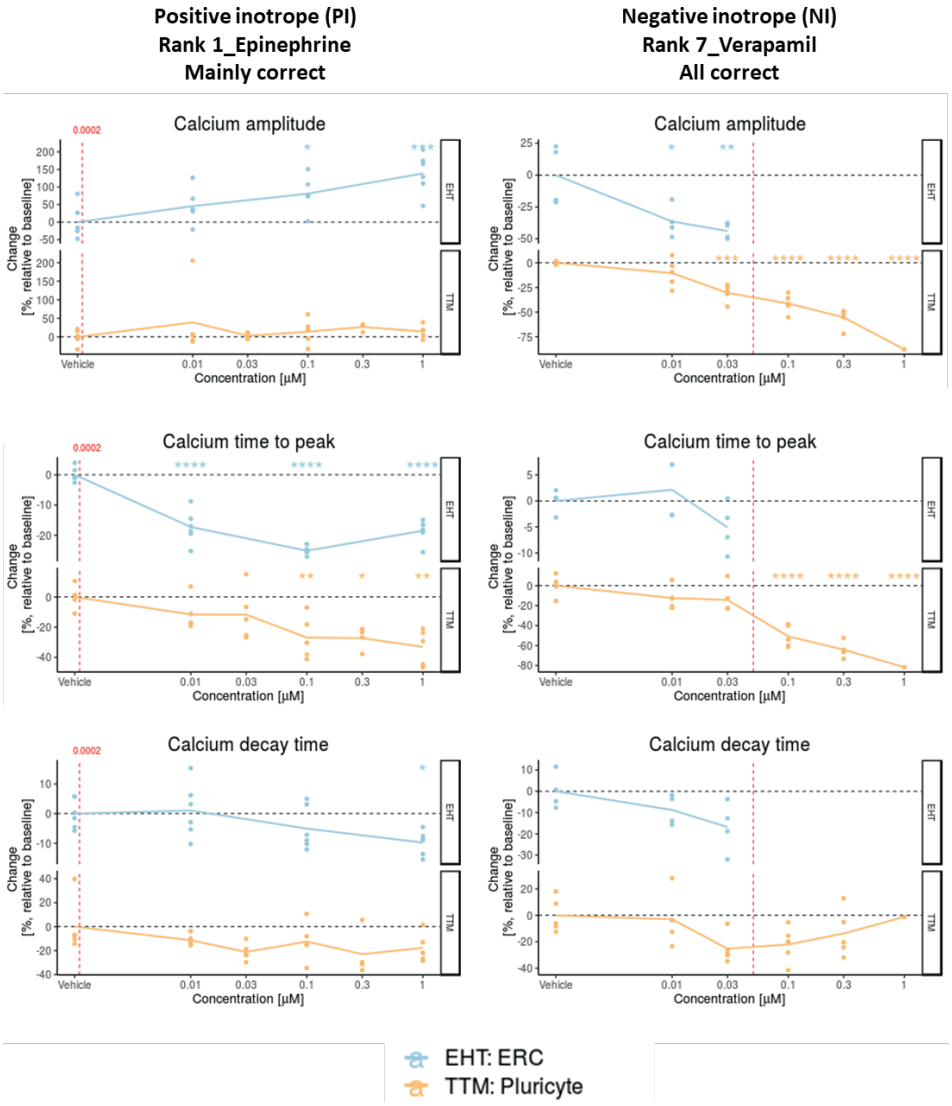

Supplementary Figure 4A: Role of Ca^{2+} analysis in prediction of inotropic response.

In some instances, Ca^{2+} transient analysis was used to guide prediction of whether a compound had a positive or negative inotropic effect. Red dotted line is free therapeutic plasma concentration (FTPC). Mainly correct: correct in most platform-cell combinations (Figure 1A), All correct: correct in all platform-cell combinations (Figure 1B). Dunnett's stats vs vehicle control: *, P<0.05; **, P<0.01; ***, P<0.001; ****, P<0.0001.

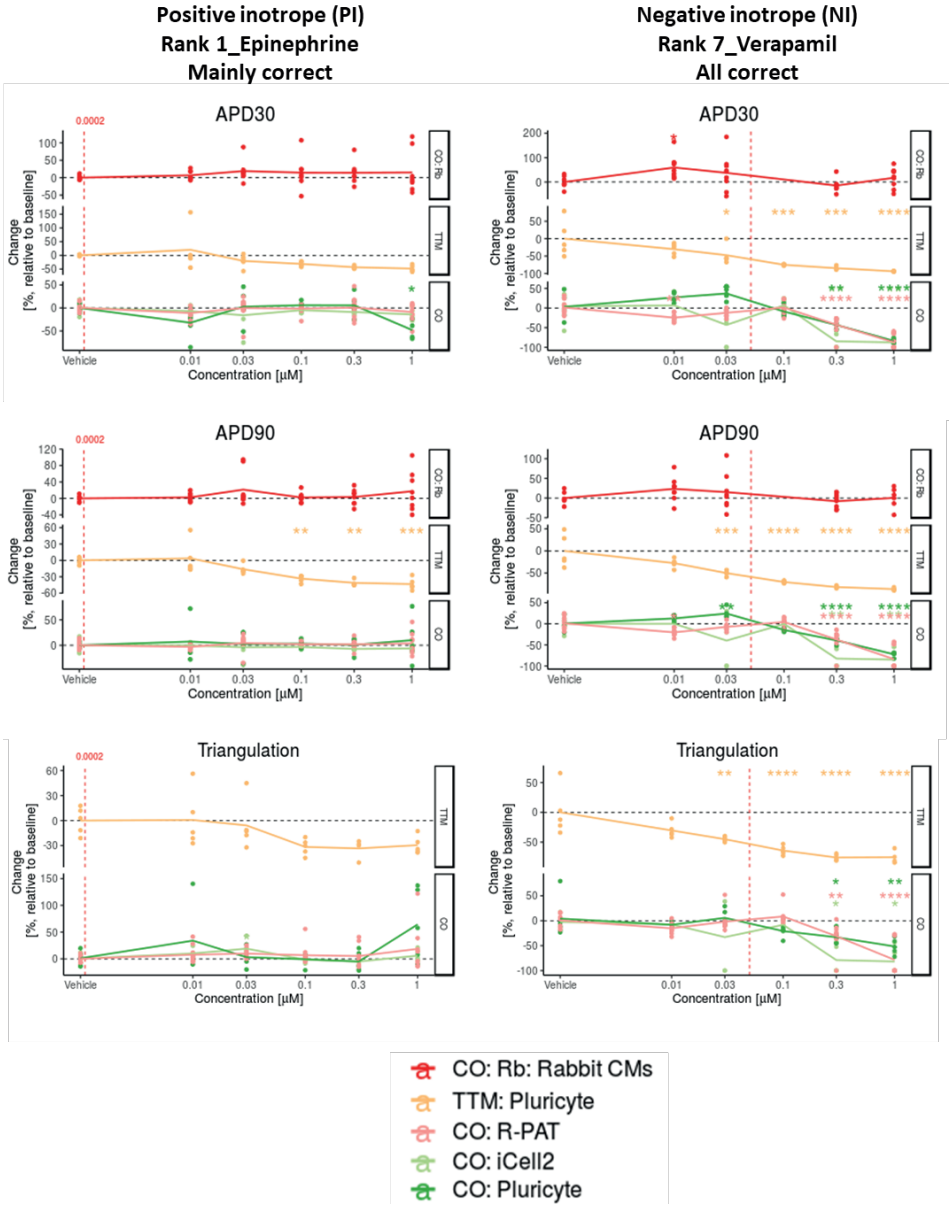

Supplementary Figure 4B: Role of voltage analysis in prediction of inotropic response.

In some instances, voltage transient analysis was used to guide prediction of whether a compound had a positive or negative inotropic effect. Red dotted line is free therapeutic plasma concentration (FTPC). Dunnett's stats vs vehicle control: *, P<0.05; **, P<0.01; ***, P<0.001; ****, P<0.0001.a

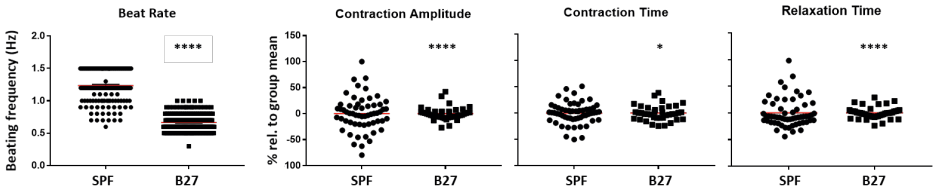

Supplementary Figure 5: Serum/protein-free medium increases spontaneous beating rates and data distribution.

Using the CO:R-PAT platform-cell combination, recordings were evaluated in hiPSC-CMs cultured as 2D monolayers in serum-/protein-free medium (SPF) versus the protein-containing medium, RPMI-B27 (B27). Culture in SPF significantly increased spontaneous beating rates (P≤ 0.0001, Mann Whitney), and increased variance of data distribution for CA, CT and RT (P≤ 0.0001, 0.05 and 0.0001, respectively; F-test for variance).

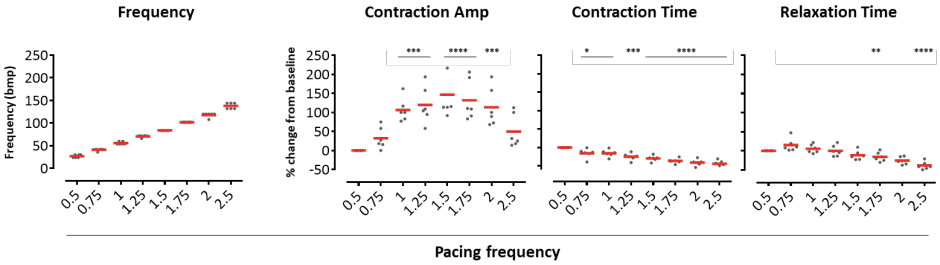

Supplementary Figure 6: Positive force frequency relationship in EHTs paced between 0.5 and 1.5 Hz.

Spontaneous beat rate of EHTs was reduced by 3 hour pre-treatment with 300 nM ivabradine, an If current inhibitor. Subsequent electrical pacing showed beating frequencies that followed the frequency of the stimulus. CA increased from 0.5 to 1.5 Hz but plateaued and declined at higher frequencies. These changes were reflected in the CT and RT data. Dunnett's stats vs vehicle control: *, P<0.05; **, P<0.01; ***, P<0.001; ****, P<0.0001.

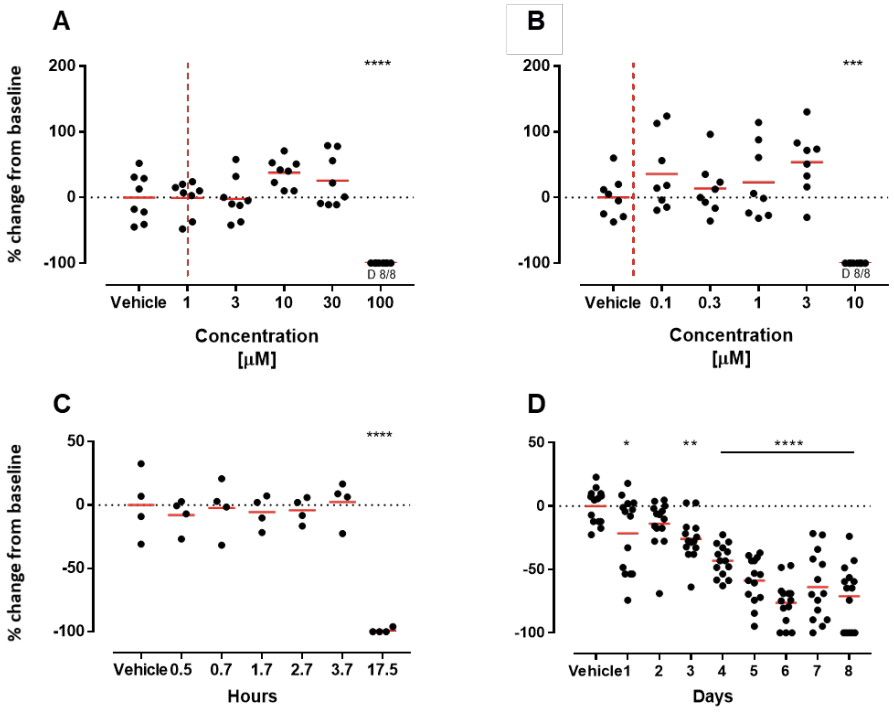

Supplementary Figure 7: Prolonged exposure detects NIs in 2D and 3D cultures of hiPSC-CMs.

Contraction amplitude (CA) was measured in the CO:R-PAT platform-cell combination exposed to various concentrations of doxorubicin (A) or sunitinib (B) for 24 hours, with the highest test concentration causing cell death. Red dotted line is free therapeutic plasma concentration (FTPC). The EHT:ERC platform-cell combination was exposed to 100 µM doxorubicin (C) or 1 µM sunitinib (D) for up to 17.5 hr (C) or up to 8 days (D). CA is shown normalized to time controls. Dunnett's stats vs vehicle control: *, P<0.05; **, P<0.01; ***, P<0.001; ****, P<0.0001.

Supplementary Table 1: Compound selection within the CRACK-IT study.

Eight training, non-blinded "Tier 1 (T1) training set" compounds with known positive or negative inotropic effects were selected to standardise the working practices across the platform-cell combinations within the study. Twenty eight "Tier 2 (T2) test set" compounds were chosen for the blinded phase of the study, of which 18 were positive inotropes (PI) or negative inotropes (NI) and span the main modes of action known to alter contractility responses of cardiomyocytes. The remainder were considered as no effect drugs (NE, no effect on cardiac contractility). A 5 x ½ log range was chosen based on the literature and/or free therapeutic plasma concentration (FTPC). Abbreviations: n.d, not defined; n.a, not applicable; PC, positive chronotropy; PI, positive inotropy; PCl, positive clinotropy; PL, positive lusitropy; NC, negative chronotropy; NI, negative inotropy; NCl, negative clinotropy; NL, negative lusitropy; inotropy is defined as change in peak force, clinotropy as change in time-to-peak force (generally from 20% above baseline to peak and "positive" being an abbreviation) and lusitropy as change in relaxation time (time from peak force generally to 80% relaxation and "positive" being an abbreviation); EC_{50}, half maximal effective concentration; IC_{50}, half maximal effective inhibitory concentration; GP, guinea pig; hERG, human eag-related gene; NCX, Na^+/Ca^{2+} exchanger; RR, blood pressure; RyR2, ryanodine receptor 2; SR, sarcoplasmic reticulum; * indicates lack of clarity in literature on inotropic effect; # in spontaneously contracting preparations.

Drug	Use	PI, NI, NE	Main mechanism of action	Expected cardiac effects in vivo	Expected effect on contractility in isolated cardiomyocytes/ heart muscles	Cellular mechanism of inotropic effect	Concentration range applied (μM)	FTPC (μM)	Refs
Isoprenaline	T1	PI	β1- and β2-adrenoceptor agonist	PI, PC	PI, PC#, PCl, PL EC_{50} 0.01 μM	Increase in cAMP, Ca^{2+} influx, SR Ca^{2+} uptake and SR load	0.0003-0.1	0.0095	(Reyes et al. 1993)
Digoxin	T1	PI	Na^+/K^+ ATPase inhibitor	PI, arrhythmias	PI+ PL (< 1 μM, slowly developing, $t_{1/2}$ conc.-dependent) NI + diast. shortening (>1 μM)	Na^+/K^+ inhibition, Ca^{2+} increase via NCX	0.01-10	0.00075-0.0015	(Lullmann and Ravens 1973)
Bay K 8644	T1	PI	L-type Ca^{2+} channel agonist	PI (indirect NC because of RR increase)	PI, NL	Increase in Ca^{2+} influx	0.03-3	n.d.	(Aass et al. 1988)

EMD 57033	T1	PI	Calcium sensitizer	PI	PI, NL, EC_{50} ~5 μM, diastolic shortening at high conc.	Myofilament sensitization to Ca^{2+}	0.01-30	16 μM	(Hajjar et al. 1997), (de Zeeuw et al. 2000)
Caffeine	T1	PI	Opener of RyR2 (at high concentration)	PI or NI o NE	Small PI and PL at 100 μM, transient large PI, NL at >10 mM	Opening of RyR2	100-10,000	20-40	(Chaban et al. 2017)
Nifedipine	T1	NI	L-type Ca^{2+} channel blocker (dihydropyridine)	Small NI (direct) overridden by adrenergic activation, PC (indirect)	NI, IC_{50} 0.1 μM	Decreased Ca^{2+} influx	0.003-0.3	0.02	(Angus et al. 2000)
Ryanodine	T1	NI	Inhibitor of RyR2	n.d.	NI, NCl, species dependent biphasic, IC_{50} ~0.01 μM	Decreased SR Ca^{2+} release	1-30	n.d.	(Sutko and Willerson 1980), (Fedorov et al. 2002)
Thapsigargin	T1	NI	Inhibitor of SR Ca^{2+} ATPase	n.d.	Heart muscle: NI ~50% at 500 μM, NL ~20% at 500 μM Isolated myocytes: ~90% NI at 0.1 μM	Decreased SR Ca^{2+} uptake and load	0.3-30	n.d.	(Kirby et al. 1992), (Baudet et al. 1993)
Epinephrine	T2	PI	Non-selective α1-, β1- and β2-adrenoceptor agonist	PI, PC	PI, PC#, PCl, PL EC_{50} 0.1 μM	Increase in cAMP, Ca^{2+} influx, SR Ca^{2+} uptake and SR load	0.01 - 1	0.0002-0.050	(Molenaar et al. 2007), (Wortsman et al. 1984)
Forskolin	T2	PI	Adenylyl cyclase stimulator	PI, PC	PI, PC#, PCl, PL EC_{50} 5-10 μM	Increase in cAMP, Ca^{2+} influx, SR Ca^{2+} uptake and SR load	0.1 - 10	0.012-0.024 (colforsin)	(Bristow et al. 1984), (Kikura et al. 2004)

Levosimendan	T2	PI	PDE3 inhibitor (IC_{50} 25 nM) Calcium sensitizer K_{ATP} channel agonist	PI, PC (more heart rate increase and RR decrease than dobutamine)	Small PI (~50%), PC#, PCl+PL (14%), EC_{50} ~0.1 µM	Increase in cAMP and myofilament sensitization to Ca^{2+}	0.01 - 1	0.026-0.35	(Boknik et al. 1997), (Hasenfuss et al. 1998), (Mebazaa et al. 2007), (Papp et al. 2012), (Orstavik et al. 2014), (Abi-Gerges et al. 2013), (Puttonen et al. 2008)
Pimobendan	T2	PI	Calcium sensitizer PDE inhibitor (partial)	PI, small PC	PI, small PC#, PL and NL at low/high conc., EC_{50} 34 µM	Increase in cAMP and myofilament sensitization to Ca^{2+}	1 - 100	0.005-0.01	(Honerjager et al. 1984), (Berger et al. 1985), (Chu et al. 1995)
Dobutamine	T2	PI	α1-, β1- and β2 adrenoceptor agonist	PI, PC, less HR-stimulation than epinephrine	PI, PC#, PCl, PL. EC_{50} 1-3 µM	Increase in cAMP, Ca^{2+} influx, SR Ca^{2+} uptake and SR load	0.1 - 10	0.07-1	(Ishihata et al. 1988), (Brown et al. 1987), (Mahoney et al. 2016)
Milrinone	T2	PI	PDE3 inhibitor	PI, PC (more heart rate increase and RR decrease than dobutamine)	Small PI, PC#, PCl, PL (smaller than ISO) EC_{50} 60 µM	Increase in cAMP, Ca^{2+} influx, SR Ca^{2+} uptake and SR load	1-100	0.1-0.15	(Brown et al. 1986), (Bailey et al. 1994)
Omecamtiv mecarbil	T2	PI	Cardiac specific myosin activator	PI, prolonged syst. ejection time, small decrease in heart rate	PI, NCl, NL, diastolic shortening (dog myocytes). EC_{50} 1 µM	Increased number of myosin heads binding to actin, no affection of Ca^{2+} transient	0.01 - 1	0.05 -0.42	(Cleland et al. 2011), (Planelles-Herrero et al. 2017), (Horvath et al. 2017), (Teerlink et al. 2011), (Liu et al. 2016)

Terbutaline	T2	PI	β2-adrenoceptor agonist	Small PI and PC	PI, PC#, PCl, PL. EC_{50} 3 μM	Increase in cAMP, Ca^{2+} influx, SR Ca^{2+} uptake and SR load	0.1 - 10	1.3	(Schafers et al. 1994), (Dyreborg et al. 2016)
Verapamil	T2	NI	L-type Ca^{2+} channel blocker, hERG blocker	NI (direct) partially masked by adrenergic activation (indirect), NC or none, ND (direct)	NI, IC_{50} 0.1 μM	Decreased Ca^{2+} influx	0.01 - 1	0.05	(Angus et al. 2000), (Giacomini et al. 1984)
Doxorubicin	T2	NI	Impairs Ca^{2+} transport mechanisms in sarcoplasmic reticulum	NI, time course of cardiotox dose-dependent	PI+NCl and reduced post-rest potentiation at 30 μM (GP), but strong NI at 1000 μM (GP, rat); rate-dependent	Complex, including increased mitochondrial ROS	0.1 - 10	1-2	(Temma et al. 1993), (Hofling and Bolte 1981), (Matsushita et al. 2000), (Danesi et al. 1999)
Sunitinib	T2	NI	Multi-targeted TK inhibitor	NI, NC at high doses, chronic cardiotox	NI, IC_{50} 10 μM	Complex	0.1 - 10	0.003	(Mooney et al. 2015), (Abi-Gerges et al. 2013), (Bello et al. 2006)
Citalopram	T2	NI	SSR inhibitor, hERG & L-type Ca^{2+} channel inhibitor	None (at therapeutic doses), higher risk of TdP	NI at 30 μM (-57% in hEHT, -38% in human atria)	Decrease in Ca^{2+} influx	1 - 100	0.05	(Witchel et al. 2002), (Mannhardt et al. 2017), (Rao 2007)
Itraconazole	T2	NI	Triazole antifungal, inhibitor of Na^{+} channels and mitochondrial voltage-dependent anion channel 1	NI	NI (-30% at 0.3 μM; rabbit heart)	Decreased Na^{+} influx (?)	0.1 - 10	0.00086 (higher in tissues)	(Head et al. 2015), (Qu et al. 2013), (Bellmann 2007)

Sorafenib	T2	NI	Multi-targeted kinase inhibitor	None or NI at high doses, delayed cardiotox	None (feline and canine CM, but cell death), NI (rat heart)	n.d.	0.1 - 10	0.03 (higher tissue levels)	(Henderson et al. 2013), (Duran et al. 2014), (Abi-Gerges et al. 2013), (Kim et al. 2013)
Ivabradine*	T2	NI	I_f inhibitor	NC (therapeutic)	None, NC at >10 µM (spontaneously beating preps), NIE (-13/-60% in guinea pig atria/PM, -38% human trabeculae at 100 µM); PI in mouse left atria and 30% of human trabeculae	Decrease in Ca^{2+} transient peak	0.1 - 10	0.01-0.1	(Perez et al. 1995), (Boldt et al. 2010), (Bois et al. 1996), (Mesirca et al. 2014), (Choi et al. 2016)
Flecainide	T2	NI	Na^+ channel blocker, hERG blocker	NI	NI, IC_{50} 0.3 µM	Decreased Na^+ influx (?)	0.1 - 10	0.2-0.4	(Abi-Gerges et al. 2013), (McQuinn et al. 1988)
Phentolamine	T2	NI	Non-selective α adrenoceptor antagonist, Na^+ and Ca^{2+} channel blocker at high conc.	PC (indirect)	NI, IC_{50} ~20 µM	Decreased Na^+ and Ca^{2+} influx	1-100	2.25	(Sada 1978), (Rosen et al. 1971)
Zimelidine*	T2	NI	SSR inhibitor	None (at ther. doses), QT and QRS widening at high doses	n.d.	n.d.	1 - 100	0.78	(Lindbom and Forsberg 1981), (Forsberg and Lindbom 1983), (Naranjo et al. 1984)
Acetylsalicylic acid	T2	NE	Cyclooxygenase inhibitor	None	None	n.a.	1 - 100	0.3-2	(Abi-Gerges et al. 2013)
Atenolol	T2	NE	β1>β2 adrenoceptor antagonist	NI, NC, ND	None (in absence of agonist) until 3000 µM (in contrast to e.g. propranolol)	n.a.	0.1 - 10	1	(Lemoine et al. 1988), (Kaumann and Blinks 1980)

Captopril	T2	NE	ACE inhibitor	None	None	n.a.	1-100	1-2	(Abi-Gerges et al. 2013), (Giudicelli et al. 1987)
Glibenclamide	T2	NE	K_{ATP} channel antagonist	None or PI in ischemia	None; PI in ischemia or presence of K_{ATP} opener; NI in adrenalectomized dogs, NE in isolated dog heart trabeculae	n.a.	0.1 - 10	0.02-0.06	(Satoh et al. 1990), (Murakami et al. 1992), (Pogatsa and Dubecz 1977), (Rydberg et al. 1997)
Enalaprilat	T2	NE	ACE inhibitor	None	None	n.a.	1 - 100	0.12	(Stage et al. 2017)
Clonidine	T2	NE	α2-adrenoceptor agonist	NI, NC	None	n.a.	0.01 - 1	0.002-0.004	(Jarrott et al. 1979), (Kleiber et al. 2017)
Paracetamol	T2	NE	Prostaglandin synthesis inhibitor	None	None	n.a.	10 - 1000	50	(Marks et al. 2012), (Kamali et al. 1993), (Brown et al. 1992)
Tolbutamide	T2	NE*	K_{ATP} channel antagonist, weak adenylyl cyclase stimulator	None or PI (dogs, men)	None (canine CM) or small PI (rabbit atria, rat heart), EC_{50} ~30 µM	Increase in cAMP (?)	1 - 100	20-30	(Levey et al. 1971), (Lasseter et al. 1972), (Abi-Gerges et al. 2013), (Whiting et al. 1981)
Pravastatin	T2	NE	HMG CoA reductase inhibitor	None	None	n.a.	1 - 100	0.018	(Costantine et al. 2016)
Sildenafil	T2	NE	PDE5 Inhibitor	None or PI+PC (indirect)	None	n.a.	0.3 - 30	0.02	(Sugiyama et al. 2001), (Walker et al. 1999)

Aass H, Skomedal T, Osnes JB. 1988. Increase of cyclic amp in subcellular fractions of rat heart muscle after beta-adrenergic stimulation: Prenalterol and isoprenaline caused different distribution of bound cyclic amp. J Mol Cell Cardiol. 20(9):847-860.

Abi-Gerges N, Pointon A, Pullen GF, Morton MJ, Oldman KL, Armstrong D, Valentin JP, Pollard CE. 2013. Preservation of cardiomyocytes from the adult heart. J Mol Cell Cardiol. 64:108-119.

Angus JA, Sarsero D, Fujiwara T, Molenaar P, Xi Q. 2000. Quantitative analysis of vascular to cardiac selectivity of l- and t-type voltage-operated calcium channel antagonists in human tissues. Clin Exp Pharmacol Physiol. 27(12):1019-1021.

Bailey JM, Levy JH, Kikura M, Szlam F, Hug CC, Jr. 1994. Pharmacokinetics of intravenous milrinone in patients undergoing cardiac surgery. Anesthesiology. 81(3):616-622.

Baudet S, Shaoulian R, Bers DM. 1993. Effects of thapsigargin and cyclopiazonic acid on twitch force and sarcoplasmic reticulum ca2+ content of rabbit ventricular muscle. Circ Res. 73(5):813-819.

Bellmann R. 2007. Clinical pharmacokinetics of systemically administered antimycotics. Curr Clin Pharmacol. 2(1):37-58.

Bello CL, Sherman L, Zhou J, Verkh L, Smeraglia J, Mount J, Klamerus KJ. 2006. Effect of food on the pharmacokinetics of sunitinib malate (su11248), a multi-targeted receptor tyrosine kinase inhibitor: Results from a phase i study in healthy subjects. Anticancer Drugs. 17(3):353-358.

Berger C, Meyer W, Scholz H, Starbatty J. 1985. Effects of the benzimidazole derivatives pimobendan and 2-(4-hydroxy-phenyl)-5-(5-methyl-3-oxo-4,5-dihydro-2h-6- pyridazinyl) benzimidazole . Hcl on phosphodiesterase activity and force of contraction in guinea-pig hearts. Arzneimittelforschung. 35(11):1668-1673.

Bois P, Bescond J, Renaudon B, Lenfant J. 1996. Mode of action of bradycardic agent, s 16257, on ionic currents of rabbit sinoatrial node cells. British journal of pharmacology. 118(4):1051-1057.

Boknik P, Neumann J, Kaspareit G, Schmitz W, Scholz H, Vahlensieck U, Zimmermann N. 1997. Mechanisms of the contractile effects of levosimendan in the mammalian heart. J Pharmacol Exp Ther. 280(1):277-283.

Boldt A, Gergs U, Ponicke K, Simm A, Silber RE, Neumann J. 2010. Inotropic effects of ivabradine in the mammalian heart. Pharmacology. 86(5-6):249-258.

Bristow MR, Ginsburg R, Strosberg A, Montgomery W, Minobe W. 1984. Pharmacology and inotropic potential of forskolin in the human heart. J Clin Invest. 74(1):212-223.

Brown L, Nabauer M, Erdmann E. 1986. The positive inotropic response to milrinone in isolated human and guinea pig myocardium. Naunyn-Schmiedeberg's archives of pharmacology. 334(2):196-201.

Brown L, Nabauer M, Erdmann E. 1987. Dobutamine: Positive inotropy by nonselective adrenoceptor agonism in isolated guinea pig and human myocardium. Naunyn Schmiedebergs Arch Pharmacol. 335(4):385-390.

Brown RD, Wilson JT, Kearns GL, Eichler VF, Johnson VA, Bertrand KM. 1992. Single-dose pharmacokinetics of ibuprofen and acetaminophen in febrile children. Journal of clinical pharmacology. 32(3):231-241.

Chaban R, Kornberger A, Branski N, Buschmann K, Stumpf N, Beiras-Fernandez A, Vahl CF. 2017. In-vitro examination of the positive inotropic effect of caffeine and taurine, the two most frequent active ingredients of energy drinks. BMC cardiovascular disorders. 17(1):220.

Choi HY, Bae KS, Cho SH, Ghim JL, Choe S, Jung JA, Lim HS. 2016. Population plasma and urine pharmacokinetics of ivabradine and its active metabolite s18982 in healthy korean volunteers. Journal of clinical pharmacology. 56(4):439-449.

Chu KM, Shieh SM, Hu OY. 1995. Pharmacokinetics and pharmacodynamics of enantiomers of pimobendan in patients with dilated cardiomyopathy and congestive heart failure after single and repeated oral dosing. Clin Pharmacol Ther. 57(6):610-621.

Cleland JG, Teerlink JR, Senior R, Nifontov EM, Mc Murray JJ, Lang CC, Tsyrlin VA, Greenberg BH, Mayet J, Francis DP et al. 2011. The effects of the cardiac myosin activator, omecamtiv mecarbil, on cardiac function in systolic heart failure: A double-blind, placebo-controlled, crossover, dose-ranging phase 2 trial. Lancet. 378(9792):676-683.

Costantine MM, Cleary K, Hebert MF, Ahmed MS, Brown LM, Ren Z, Easterling TR, Haas DM, Haneline LS, Caritis SN et al. 2016. Safety and pharmacokinetics of pravastatin used for the prevention of preeclampsia in high-risk pregnant women: A pilot randomized controlled trial. Am J Obstet Gynecol. 214(6):720 e721-720 e717.

Danesi R, Conte PF, Del Tacca M. 1999. Pharmacokinetic optimisation of treatment schedules for anthracyclines and paclitaxel in patients with cancer. Clinical pharmacokinetics. 37(3):195-211.

de Zeeuw S, Trines SA, Krams R, Duncker DJ, Verdouw PD. 2000. *In vivo* evidence that emd 57033 restores myocardial responsiveness to intracoronary ca(2+) in stunned myocardium. European journal of pharmacology. 403(1-2):99-109.

Duran JM, Makarewich CA, Trappanese D, Gross P, Husain S, Dunn J, Lal H, Sharp TE, Starosta T, Vagnozzi RJ et al. 2014. Sorafenib cardiotoxicity increases mortality after myocardial infarction. Circ Res. 114(11):1700-1712.

Dyreborg A, Krogh N, Backer V, Rzeppa S, Hemmersbach P, Hostrup M. 2016. Pharmacokinetics of oral and inhaled terbutaline after exercise in trained men. Front Pharmacol. 7:150.

Fedorov VV, Sharifov OF, Piatakova OP, Beloshapko GG, Iushmanova AV, Rozenshtraukh LV. 2002. [effects of ryanodine receptors block on spontaneous initiation of atrial fibrillation in the intact canine heart]. Kardiologiia. 42(2):59-71.

Forsberg T, Lindbom LO. 1983. Cardiovascular effects of zimelidine and tricyclic antidepressants in conscious rats. Acta Pharmacol Toxicol (Copenh). 53(3):223-229.

Giacomini KM, Massoud N, Wong FM, Giacomini JC. 1984. Decreased binding of verapamil to plasma proteins in patients with liver disease. J Cardiovasc Pharmacol. 6(5):924-928.

Giudicelli JF, Richer C, Mattei A. 1987. Pharmacokinetics and biological effects of captopril and hydrochlorothiazide after acute and chronic administration either alone or in combination in hypertensive patients. British journal of clinical pharmacology. 23 Suppl 1:51S-63S.

Hajjar RJ, DiSalvo TG, Schmidt U, Thaiyananthan G, Semigran MJ, Dec GW, Gwathmey JK. 1997. Clinical correlates of the myocardial force-frequency relationship in patients with end-stage heart failure. The Journal of heart and lung transplantation : the official publication of the International Society for Heart Transplantation. 16(11):1157-1167.

Hasenfuss G, Pieske B, Castell M, Kretschmann B, Maier LS, Just H. 1998. Influence of the novel inotropic agent levosimendan on isometric tension and calcium cycling in failing human myocardium. Circulation. 98(20):2141-2147.

Head SA, Shi W, Zhao L, Gorshkov K, Pasunooti K, Chen Y, Deng Z, Li RJ, Shim JS, Tan W et al. 2015. Antifungal drug itraconazole targets vdac1 to modulate the ampk/mtor signaling

axis in endothelial cells. Proc Natl Acad Sci U S A. 112(52):E7276-7285.
Henderson KA, Borders RB, Ross JB, Huwar TB, Travis CO, Wood BJ, Ma ZXJ, Hong SP, Vinci TM, Roche BM. 2013. Effects of tyrosine kinase inhibitors on rat isolated heart function and protein biomarkers indicative of toxicity. Journal of Pharmacological and Toxicological Methods. 68(1):150-159.
Hofling B, Bolte HD. 1981. Acute negative inotropic effect of adriamycin (doxorubicin). Naunyn-Schmiedeberg's archives of pharmacology. 317(3):252-256.
Honerjager P, Heiss A, Schafer-Korting M, Schonsteiner G, Reiter M. 1984. Ud-cg 115--a cardiotonic pyridazinone which elevates cyclic amp and prolongs the action potential in guinea-pig papillary muscle. Naunyn-Schmiedeberg's archives of pharmacology. 325(3):259-269.
Horvath B, Szentandrassy N, Veress R, Almassy J, Magyar J, Banyasz T, Toth A, Papp Z, Nanasi PP. 2017. Frequency-dependent effects of omecamtiv mecarbil on cell shortening of isolated canine ventricular cardiomyocytes. Naunyn Schmiedebergs Arch Pharmacol. 390(12):1239-1246.
Ishihata A, Kushida H, Endoh M. 1988. Enantiomers of dobutamine increase the force of contraction via beta adrenoceptors, but antagonize competitively the positive inotropic effect mediated by alpha-1 adrenoceptors in the rabbit ventricular myocardium. J Pharmacol Exp Ther. 246(3):1080-1087.
Jarrott B, Louis WJ, Summers RJ. 1979. The characteristics of [3h]-clonidine binding to an alpha-adrenoceptor in membranes from guinea-pig kidney. British journal of pharmacology. 65(4):663-670.
Kamali F, Thomas SH, Ferner RE. 1993. Paracetamol elimination in patients with non-insulin dependent diabetes mellitus. British journal of clinical pharmacology. 35(1):58-61.
Kaumann AJ, Blinks JR. 1980. Stimulant and depressant effects of beta-adrenoceptor blocking agents on isolated heart muscle. A positive inotropic effect not mediated through andrenoceptors. Naunyn-Schmiedeberg's archives of pharmacology. 311(3):205-218.
Kikura M, Takada T, Sato S. 2004. Age- and sex-specific incidence, risk, and latency period of a perioperative acute thromboembolism syndrome (pats). Thromb Haemost. 91(4):725-732.
Kim A, Dombi E, Tepas K, Fox E, Martin S, Wolters P, Balis FM, Jayaprakash N, Turkbey B, Muradyan N et al. 2013. Phase i trial and pharmacokinetic study of sorafenib in children with neurofibromatosis type i and plexiform neurofibromas. Pediatric blood & cancer. 60(3):396-401.
Kirby MS, Sagara Y, Gaa S, Inesi G, Lederer WJ, Rogers TB. 1992. Thapsigargin inhibits contraction and ca2+ transient in cardiac cells by specific inhibition of the sarcoplasmic reticulum ca2+ pump. J Biol Chem. 267(18):12545-12551.
Kleiber N, Mathot RAA, Ahsman MJ, Wildschut ED, Tibboel D, de Wildt SN. 2017. Population pharmacokinetics of intravenous clonidine for sedation during paediatric extracorporeal membrane oxygenation and continuous venovenous hemofiltration. British journal of clinical pharmacology. 83(6):1227-1239.
Lasseter KC, Levey GS, Palmer RF, McCarthy JS. 1972. The effect of sulfonylurea drugs on rabbit myocardial contractility, canine purkinje fiber automaticity, and adenyl cyclase activity from rabbit and human hearts. The Journal of clinical investigation. 51(9):2429-2434.
Lemoine H, Schonell H, Kaumann AJ. 1988. Contribution of beta 1- and beta 2-adrenoceptors of human atrium and ventricle to the effects of noradrenaline and adrenaline as assessed with (-)-atenolol. British journal of pharmacology. 95(1):55-66.
Levey GS, Palmer RF, Lasseter KC, McCarthy J. 1971. Effect of tolbutamide on adenyl cyclase in rabbit and human heart and contractility of isolated rabbit atria. J Clin Endocrinol Metab. 33(2):371-374.
Lindbom LO, Forsberg T. 1981. Cardiovascular effects of zimelidine and other antidepressant in conscious rats. Acta Psychiatr Scand Suppl. 290:380-384.
Liu LC, Dorhout B, van der Meer P, Teerlink JR, Voors AA. 2016. Omecamtiv mecarbil: A new cardiac myosin activator for the treatment of heart failure. Expert Opin Investig Drugs. 25(1):117-127.
Lullmann H, Ravens U. 1973. The time courses of the changes in contractile force and in transmembfane potentials induced by cardiac glycosides in guinea-pig papillary muscle. Br J Pharmacol. 49(3):377-390.
Mahoney L, Shah G, Crook D, Rojas-Anaya H, Rabe H. 2016. A literature review of the pharmacokinetics and pharmacodynamics of dobutamine in neonates. Pediatr Cardiol. 37(1):14-23.
Mannhardt I, Eder A, Dumotier B, Prondzynski M, Kramer E, Traebert M, Sohren KD, Flenner F, Stathopoulou K, Lemoine MD et al. 2017. Blinded contractility analysis in hipsc-cardiomyocytes in engineered heart tissue format: Comparison with human atrial trabeculae. Toxicological sciences : an official journal of the Society of Toxicology. 158(1):164-175.
Marks L, Borland S, Philp K, Ewart L, Lainee P, Skinner M, Kirk S, Valentin JP. 2012. The role of the anaesthetised guinea-pig in the preclinical cardiac safety evaluation of drug candidate compounds. Toxicol Appl Pharmacol. 263(2):171-183.
Matsushita T, Okamato M, Toyama J, Kodama I, Ito S, Fukutomi T, Suzuki S, Itoh M. 2000. Adriamycin causes dual inotropic effects through complex modulation of myocardial ca2+ handling. Jpn Circ J. 64(1):65-71.
McQuinn RL, Pentikainen PJ, Chang SF, Conard GJ. 1988. Pharmacokinetics of flecainide in patients with cirrhosis of the liver. Clinical pharmacology and therapeutics. 44(5):566-572.
Mebazaa A, Nieminen MS, Packer M, Cohen-Solal A, Kleber FX, Pocock SJ, Thakkar R, Padley RJ, Poder P, Kivikko M et al. 2007. Levosimendan vs dobutamine for patients with acute decompensated heart failure: The survive randomized trial. JAMA : the journal of the American Medical Association. 297(17):1883-1891.
Mesirca P, Alig J, Torrente AG, Muller JC, Marger L, Rollin A, Marquilly C, Vincent A, Dubel S, Bidaud I et al. 2014. Cardiac arrhythmia induced by genetic silencing of 'funny' (f) channels is rescued by girk4 inactivation. Nat Commun. 5:4664.
Molenaar P, Savarimuthu SM, Sarsero D, Chen L, Semmler AB, Carle A, Yang I, Bartel S, Vetter D, Beyerdorfer I et al. 2007. (-)-adrenaline elicits positive inotropic, lusitropic, and biochemical effects through beta2 -adrenoceptors in human atrial myocardium from nonfailing and failing hearts, consistent with gs coupling but not with gi coupling. Naunyn Schmiedebergs Arch Pharmacol. 375(1):11-28.
Mooney L, Skinner M, Coker SJ, Currie S. 2015. Effects of acute and chronic sunitinib treatment on cardiac function and calcium/calmodulin-dependent protein kinase ii. British journal of pharmacology. 172(17):4342-4354.
Murakami M, Furukawa Y, Karasawa Y, Ren LM, Takayama S, Chiba S. 1992. Inhibition by glibenclamide of negative chronotropic and inotropic responses to pinacidil, acetylcho

line, and adenosine in the isolated dog heart. Journal of cardiovascular pharmacology. 19(4):618-624.
Naranjo CA, Sellers EM, Kaplan HL, Hamilton C, Khouw V. 1984. Acute kinetic and dynamic interactions of zimelidine with ethanol. Clinical pharmacology and therapeutics. 36(5):654-660.
Orstavik O, Ata SH, Riise J, Dahl CP, Andersen GO, Levy FO, Skomedal T, Osnes JB, Qvigstad E. 2014. Inhibition of phosphodiesterase-3 by levosimendan is sufficient to account for its inotropic effect in failing human heart. Br J Pharmacol. 171(23):5169-5181.
Papp Z, Edes I, Fruhwald S, De Hert SG, Salmenpera M, Leppikangas H, Mebazaa A, Landoni G, Grossini E, Caimmi P et al. 2012. Levosimendan: Molecular mechanisms and clinical implications: Consensus of experts on the mechanisms of action of levosimendan. Int J Cardiol. 159(2):82-87.
Perez O, Gay P, Franqueza L, Carron R, Valenzuela C, Delpon E, Tamargo J. 1995. Effects of the two enantiomers, s-16257-2 and s-16260-2, of a new bradycardic agent on guinea-pig isolated cardiac preparations. British journal of pharmacology. 115(5):787-794.
Planelles-Herrero VJ, Hartman JJ, Robert-Paganin J, Malik FI, Houdusse A. 2017. Mechanistic and structural basis for activation of cardiac myosin force production by omecamtiv mecarbil. Nat Commun. 8(1):190.
Pogatsa G, Dubecz E. 1977. The direct effect of hypoglycaemic sulphonylureas on myocardial contractile force and arterial blood pressure. Diabetologia. 13(5):515-519.
Puttonen J, Kantele S, Ruck A, Ramela M, Hakkinen S, Kivikko M, Pentikainen PJ. 2008. Pharmacokinetics of intravenous levosimendan and its metabolites in subjects with hepatic impairment. Journal of Clinical Pharmacology. 48(4):445-454.
Qu Y, Fang M, Gao B, Amouzadeh HR, Li N, Narayanan P, Acton P, Lawrence J, Vargas HM. 2013. Itraconazole decreases left ventricular contractility in isolated rabbit heart: Mechanism of action. Toxicol Appl Pharmacol. 268(2):113-122.
Rao N. 2007. The clinical pharmacokinetics of escitalopram. Clinical pharmacokinetics. 46(4):281-290.
Reyes G, Schwartz PH, Newth CJ, Eldadah MK. 1993. The pharmacokinetics of isoproterenol in critically ill pediatric patients. Journal of clinical pharmacology. 33(1):29-34.
Rosen MR, Gelband H, Hoffman BF. 1971. Effects of phentolamine on electrophysiologic properties of isolated canine purkinje fibers. The Journal of pharmacology and experimental therapeutics. 179(3):586-593.
Rydberg T, Jonsson A, Karlsson MO, Melander A. 1997. Concentration-effect relations of glibenclamide and its active metabolites in man: Modelling of pharmacokinetics and pharmacodynamics. British journal of clinical pharmacology. 43(4):373-381.
Sada H. 1978. Effect of phentolamine, alprenolol and prenylamine on maximum rate of rise of action potential in guinea-pig papillary muscles. Naunyn-Schmiedeberg's archives of pharmacology. 304(3):191-201.
Satoh E, Yanagisawa T, Taira N. 1990. Specific antagonism by glibenclamide of negative inotropic effects of potassium channel openers in canine atrial muscle. Jpn J Pharmacol. 54(2):133-141.
Schafers RF, Adler S, Daul A, Zeitler G, Vogelsang M, Zerkowski HR, Brodde OE. 1994. Positive inotropic effects of the beta 2-adrenoceptor agonist terbutaline in the human heart: Effects of long-term beta 1-adrenoceptor antagonist treatment. J Am Coll Cardiol. 23(5):1224-1233.
Stage C, Jurgens G, Guski LS, Thomsen R, Bjerre D, Ferrero-Miliani L, Lyauk YK, Rasmussen HB, Dalhoff K, Consortium I. 2017. The pharmacokinetics of enalapril in relation to ces1 genotype in healthy danish volunteers. Basic Clin Pharmacol Toxicol. 121(6):487-492.
Sugiyama A, Satoh Y, Shiina H, Takahara A, Yoneyama M, Hashimoto K. 2001. Cardiac electrophysiologic and hemodynamic effects of sildenafil, a pde5 inhibitor, in anesthetized dogs. Journal of cardiovascular pharmacology. 38(6):940-946.
Sutko JL, Willerson JT. 1980. Ryanodine alteration of the contractile state of rat ventricular myocardium. Comparison with dog, cat, and rabbit ventricular tissues. Circ Res. 46(3):332-343.
Teerlink JR, Clarke CP, Saikali KG, Lee JH, Chen MM, Escandon RD, Elliott L, Bee R, Habibzadeh MR, Goldman JH et al. 2011. Dose-dependent augmentation of cardiac systolic function with the selective cardiac myosin activator, omecamtiv mecarbil: A first-in-man study. Lancet. 378(9792):667-675.
Temma K, Akera T, Chugun A, Kondo H, Hagane K, Hirano S. 1993. Comparison of cardiac actions of doxorubicin, pirarubicin and aclarubicin in isolated guinea-pig heart. European journal of pharmacology. 234(2-3):173-181.
Walker DK, Ackland MJ, James GC, Muirhead GJ, Rance DJ, Wastall P, Wright PA. 1999. Pharmacokinetics and metabolism of sildenafil in mouse, rat, rabbit, dog and man. Xenobiotica. 29(3):297-310.
Whiting B, Williams RL, Lorenzi M, Varady JC, Robins DS. 1981. Effect of naproxen on glucose metabolism and tolbutamide kinetics and dynamics in maturity onset diabetics. British journal of clinical pharmacology. 11(3):295-302.
Witchel HJ, Pabbathi VK, Hofmann G, Paul AA, Hancox JC. 2002. Inhibitory actions of the selective serotonin re-uptake inhibitor citalopram on herg and ventricular l-type calcium currents. FEBS letters. 512(1-3):59-66.
Wortsman J, Frank S, Cryer PE. 1984. Adrenomedullary response to maximal stress in humans. Am J Med. 77(5):779-784.

Supplementary Table 2: Comparison and unification of standard operating procedures for TTM, CO and EHT platforms.

In house means the conditions or assays used for hiPSC-CMs derived from in house hiPSC lines using in house differentiation methods. Commercial means use of Pluricyte and/or iCell2 hPSC-CMs that were purchased from Ncardia and Cellular Dynamics International, respectively.

	Protocol	Triple Transient Measurement (TTM)	CellOPTIQ® (CO)	Engineered Heart Tissues (EHTs)
Starting conditions	Format	96-well plate		1 million hiPSC-CMs / EHT
	Age	Thawing + 5-7 days	Thawing + 5-7 days (commercial) Differentiation time + 10 days (in house)	Differentiation time + 14-30 days
	Culture medium	Manufacturer instructions	Manufacturer instructions (commercial) Standard culture medium (in house)	Standard culture medium (in house)
	Quality control	Response to 100 nM digoxin; 30 nM nifedipine	Response to 30 nM nifedipine Cell purity >90% by a-actinin (in house) Spontaneous beat rate ≤1.5 Hz (in house)	Response to 100 nM isoprenaline and 30 nM nifedipine. Cell purity >70% by cTnT (for in house hiPSC-CMs). Minimum force: 0.1 mN
Experimental set-up	Medium	Commercial medium (serum free)	As for TTM (commercial) 1.8 mM Ca^{2+} (serum/protein free) (in house)	0.6-1 mM Ca^{2+}-modified Tyrode's soultion/DMEM (serum/protein free)
	Cell loading	ANINNE-6 plus, Rhod 3 AM and CellMask Deep Red	FluoVolt™	Lentiviral mediated expression of GCaMP6f in EHTs (transduction during EHT fabrication)
	Recording: Baselines	Paced at 1.2 Hz; 7 sec/area	Paced at 1.2-1.7 Hz; 10 sec/area	Paced at 1.5x basal rate (0.7-2.3 Hz); 10 sec/EHT
	Recording: Conc-response curves	Replicates: 5 wells/compound and 3 areas/well + time matched vehicle controls	Replicates: 5 wells/compound + time matched vehicle controls	Replicates: 6 EHTs/compound + time matched vehicle controls
		Solvent: max 0.1% DMSO; Treatment duration: 30 mins		
		Single concentration/well		Cumulative concentrations/EHT
		Paced at 1.2 Hz; 7 sec/area	Paced at 1.2-1.7 Hz; 10 sec/well	Paced at 1.5x basal rate (0.7-2.3 Hz); 10 sec/EHT
	Analysis	Analysis performed offline		Analysis performed online and offline
Follow-up	Recovery	n/a		Rest and recreation for ≥2 days in standard medium
	Additional testing	n/a		Baseline at 1.8 mM Ca^{2+}-Tyrode/DMEM (spontaneous; 20 sec/EHT), compare to prior baseline to evaluate permanent damage
	Repeat testing	No repeated use of cells		

Supplementary Table 3. Characterisation of the cell populations used relating to cardiomyocyte purity, subtype and electrophysiology

* Data taken from Cellular Dynamics International website (https://fujifilmcdi.com/products-services/icell-products/icell-cardiomyocytes2/) and/or PMID: 21890694.

‡ Ratio APD90/50, wherein a value of >1.7 predicts atrial-, 1.4-1.7 pacemaker- and <1.4 ventricular-like subtypes, as defined in PMID: 17895862.

§ Measured as (APD30–40)/(APD70–80) and assigned as described in PMID: 21890694.

Denoted: A, predicted as atrial-like; P, predicted as pacemaker-like; V, predicted as ventricular-like.

† Values given for ventricular-like cells, with subtype assignment made based on morphology of patch clamp electrophysiology waveform.

¤ Standard QC-criteria for every Pluricyte® Cardiomyocyte batch.

¥ Data from PMID: 28492526; 29925535 and/or 30416051.

Φ There have been conflicting views on the value of using single cell patch clamp as a predictor of cardiac subtypes. Depending on seeding density and other variables, the AP morphology of hiPSC-CMs may have any shape including those resembling chamber-specific subtypes (PMID: 25564842).

n.d. is not done (or not known / disclosed); IHC is immunohistochemistry; Replicates: N = biological, n = technical; All ± is SEM.

Cell Line Characterization							Assay Baseline Characterization					
			Single cell Patch Clamp									
Cell Line	**Differentiation method**	**Purity (marker[s] used)**	**Subtypes A:P:V%[Φ]**	**APD90**	**MDP**	**Spontaneous beat rate (Hz)**	**Platform**	**Cell line**	**Contraction duration**	**Contraction time**	**Relaxation time**	**Beat rate**
Pluricyte	Small molecules, no genetic modification or selection. Day of differentiation n.d.	>70% cTnT[+], of which >70% MLC2v[+¤]	n.d.	170±50; n=12	-75±5; n=12	0.5±0.2	TTM	Pluricyte	364±10 ms (N=3, n=50)	208±7 ms (N=3, n=50)	156±5 ms (N=3, n=50)	1.2 Hz (paced)
							CellOPTIQ	Pluricyte	658±6 ms (N=3, n=60)	213±6 ms (N=3, n=60)	445±7 ms (N=3, n=60)	1.2 Hz (paced)
iCell[2]	n.d.	>90% a-actinin[+]; n.d. for MLC2v[+¤]	24:22:54%; N=59[§]	415±22; n=32*[†]	-76±22; n=32[*†]	0.6±0.1; n=32[*†]		iCell[2]	414±3 ms (N=3, n=60)	146±4 ms (N=3, n=60)	267±4 ms (N=3, n=60)	1.5-1.7 Hz (paced)
R-PAT	Small molecules and growth factors, no genetic modification or selection. Day 22-35 of differentiation	>80% a-actinin[+] and/or cTnT[+]; >80% MLC2v[+¤]	4:18:78%; N=5, n=49[‡]	224±14; N=5, n=49	-62±1; N=5, n=49	n/a; triggered		R-PAT	423±4 ms (N=3, n=60)	152±2 ms (N=3, n=60)	276±4 ms (N=3, n=60)	1.2-1.5 Hz (paced
							EHT	R-PAT	499±11, N=144	183±4 ms, N=144	294±3 ms, N=144	1.0 Hz (paced)
ERC	Small molecule & growth factor based 3D[¥]. Day 22-35 of differentiation	>80% cTnT[+]; by IHC: MLC2v, high; MLC2a, low[¥]	n.d.	302±20 ms, N=11[¥]	-78±3.5 mV, N=5[¥]	n/a; triggered 1 Hz[¥]		ERC	313±2 ms, N=134	166±1 ms, N=134	148±1 ms, N=134	1.4 Hz (paced)